The Astrophysical Journal, 749:126 (17pp), 2012 April 20 doi:10.1088/0004-637X/749/2/126

EVIDENCE FOR TYPE Ia SUPERNOVA DIVERSITY FROM ULTRAVIOLET OBSERVATIONS WITH THE *HUBBLE SPACE TELESCOPE*

Xiaofeng Wang[1,2,3], Lifan Wang[2], Alexei V. Filippenko[3], Eddie Baron[4], Markus Kromer[5], Dennis Jack[6], Tianmeng Zhang[7], Greg Aldering[8], Pierre Antilogus[9], W. David Arnett[10], Dietrich Baade[11], Brian J. Barris[12], Stefano Benetti[13], Patrice Bouchet[14], Adam S. Burrows[15], Ramon Canal[16], Enrico Cappellaro[13], Raymond G. Carlberg[17], Elisa di Carlo[18], Peter J. Challis[19], Arlin P. S. Crotts[20], John I. Danziger[21], Massimo Della Valle[22,23], Michael Fink[24], Ryan J. Foley[19,62], Claes Fransson[25], Avishay Gal-Yam[26], Peter M. Garnavich[27], Chris L. Gerardy[28], Gerson Goldhaber[8], Mario Hamuy[29], Wolfgang Hillebrandt[5], Peter Höflich[28], Stephen T. Holland[30], Daniel E. Holz[31], John P. Hughes[32], David J. Jeffery[33], Saurabh W. Jha[32], Dan Kasen[34], Alexei M. Khokhlov[31], Robert P. Kirshner[19], Robert A. Knop[35], Cecilia Kozma[25], Kevin Krisciunas[2], Brian C. Lee[8], Bruno Leibundgut[36], Eric J. Lentz[37], Douglas C. Leonard[38], Walter H. G. Lewin[39], Weidong Li[3], Mario Livio[40], Peter Lundqvist[25], Dan Maoz[41], Thomas Matheson[42], Paolo A. Mazzali[5,13], Peter Meikle[43], Gajus Miknaitis[44], Peter A. Milne[10], Stefan W. Mochnacki[45], Ken'ichi Nomoto[46], Peter E. Nugent[8], Elaine S. Oran[46], Nino Panagia[40], Saul Perlmutter[8], Mark M. Phillips[47], Philip Pinto[10], Dovi Poznanski[48], Christopher J. Pritchet[49], Martin Reinecke[5], Adam G. Riess[40], Pilar Ruiz-Lapuente[16], Richard A. Scalzo[8], Eric M. Schlegel[50], Brian P. Schmidt[51], James Siegrist[8], Alicia M. Soderberg[19], Jesper Sollerman[25], George Sonneborn[30], Anthony Spadafora[8], Jason Spyromilio[36], Richard A. Sramek[52], Sumner G. Starrfield[53], Louis G. Strolger[54], Nicholas B. Suntzeff[2], Rollin C. Thomas[8], John L. Tonry[12], Amedeo Tornambe[55], James W. Truran[31], Massimo Turatto[21], Michael Turner[31], Schuyler D. Van Dyk[56], Kurt W. Weiler[57], J. Craig Wheeler[58], Michael Wood-Vasey[59], Stanford E. Woosley[60], and Hitoshi Yamaoka[61]

[1] Physics Department and Tsinghua Center for Astrophysics (THCA), Tsinghua University, Beijing 100084, China; wang_xf@mail.tsinghua.edu.cn
[2] Physics and Astronomy Department, Texas A&M University, College Station, TX 77843, USA
[3] Department of Astronomy, University of California, Berkeley, CA 94720-3411, USA
[4] Department of Physics, University of Oklahoma, Norman, OK 73019, USA
[5] Max-Planck-Institut für Astrophysik, Karl-Schwarzschild-Str. 1, 85748 Garching, Germany
[6] Hamburger Sternwarte, Gojenbergsweg 112, 21029 Hamburg, Germany
[7] National Astronomical Observatory of China, Chinese Academy of Sciences, Beijing 100012, China
[8] Lawrence Berkeley National Laboratory, Berkeley, CA 94720, USA
[9] Laboratoire de Physique Nucleaire des Hautes Energies, Paris, France
[10] Steward Observatory, University of Arizona, Tucson, AZ 85721, USA
[11] European Southern Observatory, 85748 Garching bei München, Germany
[12] Institute for Astronomy, University of Hawaii, Honolulu, HI 96822, USA
[13] Osservatorio Astronomico di Padova, 35122 Padova, Italy
[14] CEA/DSM/DAPNIA/Service d'Astrophysique, 91191 Gif-sur-Yvette Cedex, France
[15] Department of Astrophysical Sciences, Princeton University, Princeton, NJ 08544, USA
[16] Department d'Astronomia i Meterorologia, Universidad de Barcelona, Barcelona 8007, Spain
[17] Department of Astronomy and Astrophysics, University of Toronto, Toronto, ON M5S 3J3, Canada
[18] INAF, Osservatorio Astronomico di Teramo, 64100 Teramo, Italy
[19] Harvard/Smithsonian Center Astrophysics, Cambridge, MA 02138, USA
[20] Department of Astronomy, Columbia University, New York, NY 10025, USA
[21] INAF, Osservatorio Astronomico di Trieste, I-34143 Trieste, Italy
[22] Capodimonte Astronomical Observatory, INAF-Napoli, I-80131 Napoli, Italy
[23] International Center for Relativistic Astrophysics, I-65122 Pescara, Italy
[24] Institut für Theoretische Physik und Astrophysik, Universität Würzburg, Am Hubland, D-97074 Würzburg, Germany
[25] Stockholm University, SE-106 91 Stockholm, Sweden
[26] Department of Particle Physics and Astrophysics, Faculty of Physics, Weizmann Institute of Science, Rehovot 76100, Israel
[27] Department of Physics, University of Notre Dame, Notre Dame, IN 46556, USA
[28] Department of Physics, Florida State University, Tallahassee, FL 32306, USA
[29] Departamento de Astronomia, Universidad de Chile, Casilla 36D, Santiago, Chile
[30] Laboratory for Observational Cosmology, NASA Goddard Space Flight Center, Code 665, Greenbelt, MD 20771, USA
[31] Enrico Fermi Institute, Department of Physics, and Kavli Institute for Cosmological Physics, University of Chicago, Chicago, IL 60637, USA
[32] Department of Physics and Astronomy, Rutgers, the State University of New Jersey, Piscataway, NJ 08854, USA
[33] Department of Physics and Astronomy, Northern Arizona University, Flagstaff, AZ 86011, USA
[34] Department of Physics, University of California, Berkeley, CA 94720, USA
[35] Department of Physics, Quest University Canada, Squamish, BC, Canada
[36] European Southern Observatory, 85748 Garching bei München, Germany
[37] Department of Physics and Astronomy, University of Tennessee, Knoxville, TN 37996, USA
[38] Department of Astronomy, San Diego State University, San Diego, CA 92182, USA
[39] Massachusetts Institute of Technology, Cambridge, MA 02139, USA
[40] Space Telescope Science Institute, Baltimore, MD 21218, USA
[41] Wise Observatory, Tel Aviv University, 69978 Tel Aviv, Israel
[42] National Optical Astronomy Observatory, Tucson, AZ 85719, USA
[43] Imperial College of Science Technology and Medicine, London SW7 2AZ, UK
[44] Center for Neighborhood Technology, 2125 West North Avenue, Chicago, IL 60647, USA
[45] Department of Astronomy and Astrophysics, University of Toronto, Toronto, ON M5S 3G4, Canada
[46] IPMU, University of Tokyo, Kashiwa, Chiba 277-8583, Japan
[47] Carnegie Institution of Washington, Washington, DC 20005, USA

[48] School of Physics and Astronomy, Tel Aviv University, Tel Aviv 69978, Israel
[49] Department of Physics and Astronomy, University of Victoria, Victoria, BC V8W 2Y2, Canada
[50] Physics & Astronomy Department, University of Texas at San Antonio, San Antonio, TX 78249, USA
[51] Research School of Astronomy and Astrophysics, Australian National University, Canberra ACT 0200, Australia
[52] National Radio Astronomy Observatory, PO BoX O, Socorro, NM 87801, USA
[53] School of Earth and Space Exploration, Arizona State University, Tempe, AZ 85287, USA
[54] Department of Physics and Astronomy, Western Kentucky University, Bowling Green, KY 42101, USA
[55] INAF, Rome Astronomical Observatory, 00136 Roma, Italy
[56] IPAC, California Institute of Technology, Pasadena, CA 91125, USA
[57] Naval Research Laboratory, Washington, DC 20375, USA
[58] Department of Astronomy and McDonald Observatory, University of Texas, Austin, TX 78712, USA
[59] Pittsburgh Particle Physics, Astrophysics, and Cosmology Center (Pitt-PACC), University of Pittsburgh, Pittsburgh, PA 15260, USA
[60] Department of Astronomy and Astrophysics, University of California, Santa Cruz, CA 95060, USA
[61] Graduate School of Sciences, Kyushu University, Fukuoka 812-8581, Japan
Received 2011 October 26; accepted 2012 February 6; published 2012 March 30

ABSTRACT

We present ultraviolet (UV) spectroscopy and photometry of four Type Ia supernovae (SNe 2004dt, 2004ef, 2005M, and 2005cf) obtained with the UV prism of the Advanced Camera for Surveys on the *Hubble Space Telescope*. This data set provides unique spectral time series down to 2000 Å. Significant diversity is seen in the near-maximum-light spectra (∼2000–3500 Å) for this small sample. The corresponding photometric data, together with archival data from *Swift* Ultraviolet/Optical Telescope observations, provide further evidence of increased dispersion in the UV emission with respect to the optical. The peak luminosities measured in the uvw1/F250W filter are found to correlate with the *B*-band light-curve shape parameter $\Delta m_{15}(B)$, but with much larger scatter relative to the correlation in the broadband *B* band (e.g., ∼0.4 mag versus ∼0.2 mag for those with 0.8 mag $< \Delta m_{15}(B) <$ 1.7 mag). SN 2004dt is found as an outlier of this correlation (at $> 3\sigma$), being brighter than normal SNe Ia such as SN 2005cf by ∼0.9 mag and ∼2.0 mag in the uvw1/F250W and uvm2/F220W filters, respectively. We show that different progenitor metallicity or line-expansion velocities alone cannot explain such a large discrepancy. Viewing-angle effects, such as due to an asymmetric explosion, may have a significant influence on the flux emitted in the UV region. Detailed modeling is needed to disentangle and quantify the above effects.

Key words: cosmology: observations – distance scale – dust, extinction – supernovae: general – ultraviolet: general

Online-only material: color figures

1. INTRODUCTION

The utility of Type Ia supernovae (SNe Ia; see Filippenko 1997 for a review of SN spectral classification) as cosmological probes depends on the degree of our understanding of SN Ia physics and on various systematic effects such as cosmic chemical evolution. There is increasing evidence showing that even the so-called Branch-normal SNe Ia (Branch et al. 1993) exhibit diversity in their spectral features and light-curve shapes that do not correlate with light-curve parameters such as the decline rate (Phillips 1993; Benetti et al. 2005; Branch et al. 2009; Wang et al. 2009a; Zhang et al. 2010; Höflich et al. 2010). For example, it has been recently shown that SNe Ia having the same light-curve shape parameter such as $\Delta m_{15}(B)$ (Phillips 1993) but faster expanding ejecta are on average ∼0.1 mag redder in $B-V$ color near maximum light (Wang et al. 2009a, hereafter W09a). Possible origins of such a color difference include a change of the dust obscuring the SN (e.g., circumstellar dust versus interstellar dust; W09a), an effect of line blanketing (Foley & Kasen 2011), or a projection effect in an asymmetric explosion (Maeda et al. 2011). Moreover, the peak luminosity of SNe Ia seems to show an additional dependence on the global characteristics of their host galaxies: events of the same light-curve shape and color may be ∼0.1 mag brighter in massive (presumably metal-rich) host galaxies (Kelly et al. 2010; Sullivan et al. 2010; Lampeitl et al. 2010). This correlation might also indicate variations in the explosion physics and/or differences of the progenitors in a range of environments.

Ultraviolet (UV) observations are of particular importance in understanding both the diversity of SNe Ia and their physical evolution from low to high redshifts. In conjunction with existing optical and near-infrared data, UV observations improve the determination of the bolometric light curves of SNe Ia. The UV spectrum at early times forms mainly in the outer shells of the explosion ejecta where the unburned outer layers of the white dwarf play a large role in shaping the appearance of the spectrum. The dependence of the UV emission on the progenitor metallicity has been theoretically studied by several authors (Pauldrach et al. 1996; Höflich et al. 1998; Mazzali 2000; Lentz et al. 2000; Timmes et al. 2003; Sauer et al. 2008). Both Höflich et al. (1998) and Sauer et al. (2008) argued that increasing the metallicity in the outer layers would lead to a stronger UV flux, with the latter highlighting the contribution from the reverse-fluorescence scattering of photons from red to blue wavelengths. In contrast to the above studies, Lentz et al. (2000) predicted that increasing the metallicity of the progenitor should cause a decrease in the level of the UV pseudocontinuum due to a decrease in the line opacity and cooling. A much larger effect was proposed by Timmes et al. (2003), who argued for a significant increase of ^{56}Ni, and hence of the resulting luminosity, with increasing metallicity (but see Howell et al. 2009). We note that current theories do not offer a consensus picture as to the effects of changing metallicity on the overall UV flux. UV observations of a large sample of SNe Ia are needed to help quantify the UV properties and constrain the above models.

The necessity of observing above Earth's atmosphere has resulted in a sparse UV data set for low-redshift SNe Ia; see

[62] Clay Fellow.

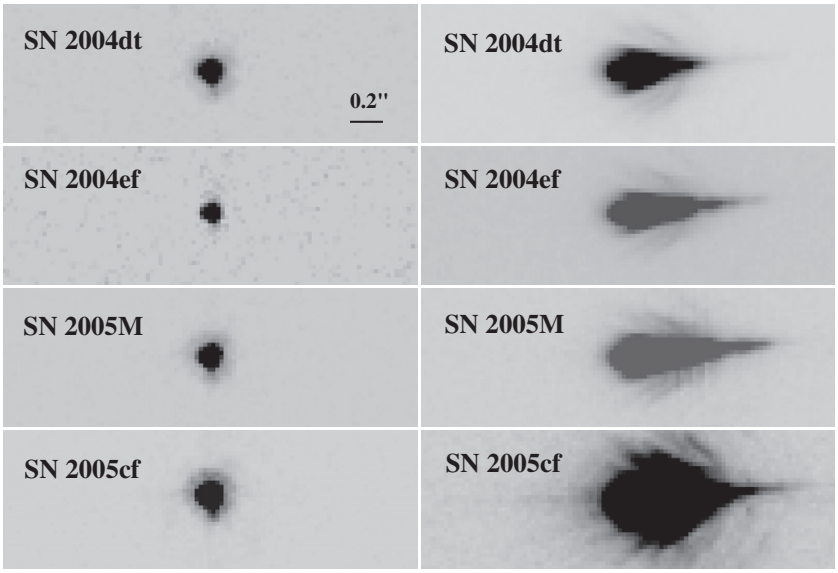

Figure 1. Left panels: direct images (F330W) of SNe 2004dt, 2004ef, 2005M, and 2005cf near maximum light obtained with *HST* ACS/HRC. Right panels: raw images near maximum light obtained in the ACS/HRC PR200L slitless spectroscopy mode. The dispersed image is only a few times longer than the point-spread function of the direct images, indicating that the *HST* prism spectra have very low resolution.

Panagia (2003, 2007) and Foley et al. (2008) for summaries of *International Ultraviolet Explorer* (*IUE*) and *Hubble Space Telescope (HST)* spectra. Recently, the *Swift* satellite obtained UV photometry of nearby SNe Ia (Milne et al. 2010; Brown et al. 2010), as well as some UV grism spectra (Bufano et al. 2009; Foley et al. 2011). With the successful repair of the Space Telescope Imaging Spectrograph (STIS) on board *HST* during the 2009 Servicing Mission 4, obtaining UV spectra with STIS has also become possible (Cooke et al. 2011). Observations of distant SNe Ia (with ground-based telescopes) provide larger samples that probe the UV spectral properties at high redshift (e.g., Ellis et al. 2008; Sullivan et al. 2009; Foley et al. 2012), since the rest-frame spectrum in the UV shifts to that in the optical region due to cosmic expansion. All of these data sets suggest significant dispersion in the UV for SNe Ia at both low and high redshifts. However, precise evolutionary constraints are still limited by the absence of high-quality, low-redshift UV spectral data.

In *HST* Cycle 13 (year 2004–2005), extensive UV observations of low-redshift SNe Ia were conducted (program GO-10182; PI: Filippenko). Unfortunately, with the failure of STIS shortly before the project started, the PR200L prism became the only available element on *HST* capable of UV spectroscopic observations, yielding only low-resolution but still useful UV spectra of four SNe Ia (SNe 2004dt, 2004ef, 2005M, and 2005cf). These four objects represent three different subclasses of SNe Ia. Among our sample, SN 2004dt, and perhaps SN 2004ef, can be put into the high-velocity (W09a) or the high-velocity-gradient groups (Benetti et al. 2005). Moreover, SN 2004dt has the highest line polarization ever observed in an SN Ia (Wang et al. 2006a) and is a clear outlier in the relationship between the Si II velocity gradient and the nebular-phase emission-line velocity shift (Maeda et al. 2010). SN 2005M is a spectroscopically peculiar object like SN 1991T (Filippenko et al. 1992b; Phillips et al. 1992), with the early spectrum showing weak Ca II H&K lines and prominent Fe III lines (Thomas 2005). And SN 2005cf has been regarded as a standard SN Ia (e.g., Wang et al. 2009b, hereafter W09b), belonging to the "Normal" or the low-velocity-gradient group. Our *HST* UV observations of the above four events reveal significant diversity of the UV properties among SNe Ia. Good understanding of the UV diversity forms the basis for further improvements in the application of SNe Ia as cosmological probes.

This paper is structured as follows. Observations and data reduction are described in Section 2, while Section 3 presents our results and a comparison with the existing UV data. Discussions are given in Section 4, and we summarize our conclusions in Section 5.

2. OBSERVATIONS AND DATA REDUCTION

UV observations of SNe 2004dt, 2004ef, 2005M, and 2005cf were performed using the Advanced Camera for Surveys (ACS) high-resolution channel (HRC) in both the slitless prism spectroscopy and the direct imaging modes, as shown in Figure 1. Observations with the HRC PR200L generally consist of a "direct" or undispersed image taken through the F330W filter, used to establish the zero point of the wavelength scale, and followed by dispersed images with one or more exposures through the PR200L prism. The parallel imaging observations were made through the F220W, F250W, and F330W filters, with the exposure time split into several segments. Individual exposures were combined using the MultiDrizzle task within the Space Telescope Science Data Analysis System (STSDAS) to reject cosmic rays and perform geometric-distortion corrections. A log of the observations is given in Table 1, listing the exposure time of each prism spectrum.

The UV spectra were extracted in PyRAF using the "aXe" slitless spectroscopy reduction package (Kümmel et al. 2004, 2009). The spectral extraction within aXe relies on the position, morphology, and photometry of the targets as observed in the accompanying direct image. Note that the dispersion of the PR200L prism varies with wavelength in a highly nonlinear fashion. For example, the spectral resolution is 5 Å pixel^{-1} at 1800 Å and 105 Å pixel^{-1} at 3500 Å, and it decreases rapidly to ∼563 Å pixel^{-1} by 5000 Å; see Table 4 of Larsen et al. (2006) for a detailed dispersion–wavelength relation for the PR200L prism data. The rapidly decreasing dispersion toward

Table 1
Journal of *HST* ACS PR200L Spectroscopic Observations of Type Ia Supernovae

SN	UT Date	JD[a]	Phase[b]	Exp. (s)
SN 2004dt	2004 Aug 20	3237.8	−2.0	350
SN 2004dt	2004 Aug 23	3240.6	+0.8	350
SN 2004dt	2004 Aug 27	3245.1	+5.3	350
SN 2004dt	2004 Aug 31	3249.2	+9.4	350
SN 2004dt	2004 Sep 1	3250.2	+10.4	470
SN 2004dt	2004 Sep 6	3255.2	+15.4	350
SN 2004dt	2004 Sep 7	3255.8	+16.0	490
SN 2004dt	2004 Sep 12	3260.8	+21.0	360
SN 2004dt	2004 Sep 16	3265.1	+25.3	360
SN 2004dt	2004 Sep 21	3269.9	+30.1	360
SN 2004dt	2004 Sep 27	3275.8	+36.0	360
SN 2004dt	2004 Oct 2	3281.3	+41.5	720
SN 2004dt	2004 Oct 10	3289.1	+49.3	1080
SN 2004ef	2004 Sep 14	3263.1	−1.5	1050
SN 2004ef	2004 Sep 18	3267.3	+2.7	1050
SN 2004ef	2004 Sep 22	3270.8	+6.2	1050
SN 2004ef	2004 Sep 25	3273.9	+9.3	1050
SN 2004ef	2004 Sep 29	3277.9	+13.3	360
SN 2004ef	2004 Oct 2	3281.4	+17.0	360
SN 2004ef	2004 Oct 8	3287.2	+22.6	240
SN 2004ef	2004 Oct 14	3293.1	+28.5	240
SN 2005M	2005 Jan 31	3402.0	−2.8	2760
SN 2005cf	2005 Jun 3	3525.0	−8.8	480
SN 2005cf	2005 Jun 5	3527.2	−6.6	480
SN 2005cf	2005 Jun 7	3529.3	−4.5	480
SN 2005cf	2005 Jun 11	3533.0	−0.8	720
SN 2005cf	2005 Jun 14	3536.0	+2.2	720
SN 2005cf	2005 Jun 16	3537.9	+4.1	720
SN 2005cf	2005 Jun 21	3542.6	+8.8	1680
SN 2005cf	2005 Jun 25	3547.2	+13.4	840
SN 2005cf	2005 Jun 26	3547.9	+14.1	840
SN 2005cf	2005 Jun 29	3551.2	+17.4	840
SN 2005cf	2005 Jun 30	3551.7	+17.9	840
SN 2005cf	2005 Jul 5	3557.0	+23.2	1680

Notes.
[a] Julian Date minus 2,450,000.
[b] Days relative to the epoch of the *B*-band maximum.

longer wavelengths results in an extreme "red pile-up" effect for the PR200L data (with flux at wavelengths longer than 4000 Å being compressed into just a few pixels), making studies of intrinsically red objects problematic (see the discussion in Section 3.2). To decrease the contamination of red light toward shorter wavelengths, we chose a proper extraction window by taking advantage of the fact that the diffraction spikes from the red pile-up are at an angle to the dispersion.

In the reduction of the direct images, we performed aperture photometry on the drizzled images using an aperture radius of 4 pixels (∼0.″1) to get the optimal signal-to-noise ratio (S/N). Inspection of the *HST* ACS images taken with the HRC (with a spatial resolution ∼0.″025 pixel^{-1}) shows that there is no significant emission from the diffuse source (see Figure 1); thus, we assume that the contamination of the host galaxy can be neglected for our UV photometry. The sky background level was determined from the median counts in an annulus of radius of 100–130 pixels. The measured magnitudes were further corrected to an infinite-radius aperture and placed on the Vega magnitude system (Sirianni et al. 2005). The aperture corrections from ∼0.″1 to an infinite aperture are 0.41 mag, 0.38 mag, and 0.35 mag for the F220W, F250W, and F330W filters, respectively. The photometric calibration of ACS/HRC was obtained with the observations of several spectrophotometric standards and has an uncertainty better than 2% (Pavlovsky et al. 2004), which we adopt as the uncertainty for our UV photometry.

Sources of error in obtaining absolute photometry include uncertainties in the red-leak correction and the *K*-correction. The red-leak effect, a common feature of UV filters, is contamination from an off-band flux in the red part of the spectrum. For stars with known colors or spectral types, this effect can be accurately quantified (Pavlovsky et al. 2004; Chiaberge & Sirianni 2007; Brown et al. 2010). The red-leak correction is negligible for filter F330W and is very small for filter F250W (e.g., $\lesssim$2% for stars with colors bluer than the G type). This correction is greater for filter F220W because of a significant off-band flux contamination in this band,[63] ranging from ∼2% for an A-type star (corresponding to an SN Ia at early phases) to ∼12% for a G-type star (corresponding to an SN Ia in the nebular phase). Despite the fact that all of our SNe Ia have low redshifts, *K*-corrections (Oke & Sandage 1968) are non-negligible in the UV due to a large variation in the spectral flux at shorter wavelengths. In calculating the *K*- and red-leak corrections for the UV photometry, we have used the corresponding PR200L prism spectrum mangled to match with the observed photometry (see Section 3.2) or a template from Hsiao et al. (2007) when the prism spectrum has extremely low quality or is not available. Uncertainties in the above two corrections can be derived from the fluctuations of the input spectra, which are determined by the photometric errors (for the mangled prism spectra) or are taken to be ∼10% of the flux (for the template spectrum from Hsiao et al.). The final *HST* ACS UV magnitudes of SNe 2004dt, 2004ef, and 2005M, as well as the corresponding *K*- and red-leak corrections, are listed in Table 2; corresponding data for SN 2005cf have been published by W09b.

The distances to the SNe were computed by using the recession velocity v of their host galaxies (see Table 3), with a Hubble constant $H_0 = 74$ km s^{-1} Mpc^{-1} (Riess et al. 2009). For objects in the Hubble flow ($v_{\rm helio} \gtrsim 3000$ km s^{-1}; SNe 2004dt, 2004ef, and 2005M), the recession velocity was determined with respect to the 3 K cosmic microwave background radiation; for the nearby sample with $v_{\rm helio} < 3000$ km s^{-1} (SN 2005cf), the velocity was corrected to a 220 km s^{-1} Virgocentric infall.

3. RESULTS

3.1. Ultraviolet Light Curves

Figure 2 shows the UV light curves of SNe 2004dt, 2004ef, and 2005M obtained with the *HST* ACS and the F220W, F250W, and F330W filters. Also plotted are the corresponding optical light curves (in *BVI*) from Ganeshalingam et al. (2010). As SN 2005cf was well observed and is judged to be a normal SN Ia, and its light curves have been published elsewhere (W09b), we use it as a template SN Ia for comparison study. To account for effects of the redshift on the observed SN flux, we applied *K*-corrections (Oke & Sandage 1968) to all of the light curves using the observed spectra (as shown in Figures 5 and 6) and the Hsiao et al. (2007) template.

[63] Following Chiaberge & Sirianni (2007), the cutoff wavelength between in-band and off-band is chosen as a filter's 1% transmission point, which occurs at 2860 Å, 3420 Å, and 3710 Å for F220W, F250W, and F330W, respectively.

Table 2
HST ACS Ultraviolet Photometry of Type Ia Supernovae

UT Date	JD[a]	Phase[b]	F220W (mag)	F250W (mag)	F330W (mag)	RC_{F220W} (mag)	RC_{F250W} (mag)	K_{F220W} (mag)	K_{F250W} (mag)	K_{F330W} (mag)
					SN 2004dt					
2004 Aug 20	3237.76	−2.04	17.40(03)	15.72(03)	14.45(02)	0.03(01)	0.01(01)	0.04(01)	0.11(01)	0.02(01)
2004 Aug 23	3240.68	+0.88	17.68(02)	15.97(03)	14.65(02)	0.03(01)	0.01(01)	0.05(01)	0.11(01)	0.04(01)
2004 Aug 27	3245.15	+5.35	18.16(03)	16.61(03)	15.30(02)	0.02(01)	0.01(01)	0.05(01)	0.10(01)	0.06(02)
2004 Aug 31	3249.25	+9.45	18.65(03)	17.24(02)	15.95(02)	0.02(01)	0.01(01)	0.07(01)	0.10(01)	0.06(02)
2004 Sep 1	3250.18	+10.38	18.71(03)	17.27(02)	16.09(02)	0.02(01)	0.01(01)	0.07(01)	0.10(01)	0.06(02)
2004 Sep 6	3255.18	+15.38	19.25(03)	18.06(03)	16.88(02)	0.01(01)	0.01(01)	0.06(01)	0.09(01)	0.07(02)
2004 Sep 7	3255.85	+16.05	19.31(03)	18.22(03)	17.14(03)	0.01(01)	0.01(01)	0.06(01)	0.08(01)	0.07(02)
2004 Sep 12	3260.78	+20.98	19.88(03)	18.89(02)	17.89(02)	0.01(01)	0.01(01)	0.06(01)	0.08(01)	0.07(02)
2004 Sep 16	3265.11	+25.31	20.08(03)	19.25(03)	18.38(02)	0.01(01)	0.01(01)	0.03(01)	0.07(02)	0.07(02)
2004 Sep 21	3269.92	+30.12	20.26(03)	19.59(03)	18.70(02)	0.01(01)	0.01(01)	0.03(01)	0.06(02)	0.06(01)
2004 Sep 27	3275.85	+36.05	20.55(03)	20.08(03)	19.07(02)	0.01(01)	0.01(01)	0.04(01)	0.07(02)	0.06(01)
2004 Oct 2	3281.34	+41.54	20.88(03)	20.39(03)	19.33(03)	0.01(01)	0.01(01)	0.05(04)	0.06(02)	0.07(01)
2004 Oct 10	3289.10	+49.30	21.13(03)	20.55(03)	19.48(03)	0.01(01)	0.01(01)	0.02(02)	0.06(01)	0.06(01)
					SN 2004ef					
2004 Sep 13	3262.23	−1.87	...	19.06(03)	16.98(02)	0.08(07)	0.02(01)	...	0.19(04)	0.07(03)
2004 Sep 18	3266.83	+2.94	21.62(06)	19.57(03)	17.71(02)	0.04(02)	0.02(01)	0.22(14)	0.17(02)	0.10(01)
2004 Sep 21	3270.32	+6.41	21.85(06)	19.87(03)	18.12(03)	0.04(02)	0.02(01)	0.18(09)	0.17(03)	0.13(01)
2004 Sep 24	3273.33	+9.41	22.15(09)	20.31(03)	18.59(03)	0.05(03)	0.02(01)	0.15(05)	0.17(03)	0.13(01)
2004 Sep 28	3277.43	+13.54	22.12(03)	20.52(02)	19.04(02)	0.06(04)	0.02(01)	0.08(02)	0.17(02)	0.13(01)
2004 Oct 2	3281.08	+17.13	22.58(04)	20.93(02)	19.60(02)	0.04(03)	0.02(01)	0.19(05)	0.20(07)	0.12(02)
2004 Oct 8	3286.77	+22.88	...	21.27(03)	20.23(02)	0.02(05)	0.01(01)	...	0.10(04)	0.10(02)
2004 Oct 14	3292.66	+28.79	...	21.74(03)	20.66(03)	0.01(05)	0.01(01)	...	0.09(04)	0.13(02)
					SN 2005M					
2005 Jan 28	3398.48	−6.29	20.07(02)	17.54(02)	16.02(03)	0.02(02)	0.01(01)	0.13(11)	0.13(03)	0.01(01)
2005 Jan 31	3401.60	−3.30	19.91(02)	17.45(04)	15.88(02)	0.03(02)	0.01(01)	0.15(10)	0.12(02)	0.02(01)
2005 Feb 4	3405.97	+1.23	19.96(02)	...	15.93(03)	0.02(02)	...	0.06(05)	...	0.05(01)
2005 Feb 9	3410.70	+5.96	20.57(03)	...	16.51(03)	0.02(02)	...	0.06(01)	...	0.07(02)
2005 Feb 13	3414.90	+10.16	20.87(03)	...	16.85(03)	0.02(02)	...	0.08(02)	...	0.09(01)
2005 Feb 17	3419.29	+14.49	20.82(03)	...	17.35(03)	0.02(02)	...	0.07(01)	...	0.11(03)

Notes. Uncertainties, in units of 0.01 mag, are 1σ. See W09b for *HST* UV photometry of SN 2005cf.
[a] Julian Date minus 2,450,000.
[b] Relative to the epoch of the *B*-band maximum.

The light curves have also been corrected for reddening in the host galaxy, as well as in the Milky Way (MW). The total reddening toward an SN Ia can be derived from an empirical relation established between decline rate $\Delta m_{15}(B)$ and color indexes for a low-reddening sample (e.g., W09b, and references therein). By comparing the observed color with that predicted by the $\Delta m_{15}(B)$ versus $(B_{max} - V_{max})$ relation, we estimate the total reddening $E(B-V)_{total}$ as 0.10 mag for SN 2004dt, 0.17 for SN 2004ef, 0.12 mag for SN 2005M, and 0.20 mag for SN 2005cf, with a typical error of ∼0.04 mag. The absorption in the MW was estimated by using the reddening maps of Schlegel et al. (1998) and the Cardelli et al. (1989) reddening law with $R_V = 3.1$, while extinction in the host galaxy was corrected applying an extinction law with $R_V \approx 2.3$ (e.g., Riess et al. 1996; Reindl et al. 2005; Wang et al. 2006b; Kessler et al. 2009). Since all four SNe Ia have low host-galaxy reddening (e.g., $E(B-V)_{host} \lesssim 0.10$ mag), a moderate change of the extinction-law coefficient will have limited effect on the UV light curves shown in Figure 2. According to the extinction-law coefficients recalculated by Brown et al. (2010), a change in R_V from 1.8 (LMC dust) to 3.1 (MW dust) will only result in a difference of ∼0.02 mag in F330W and ≲0.15 mag in F250W for an SN Ia with a host-galaxy reddening $E(B-V)_{host} = 0.10$ mag. Note, however, that the magnitude change in F220W could be larger due to a dramatic variation in the resultant extinction coefficient R_{F220W}. Table 3 lists the relevant parameters of these four SNe Ia.

One can see from Figure 2 that the UV light curves of our SNe Ia show a large dispersion, especially at shorter wavelengths, while the optical counterparts are generally similar except in the *I* band where there is more diversity. Of our sample, SN 2004ef appears relatively faint in all bands, consistent with the fact that it is a slightly faster decliner with $\Delta m_{15}(B) \approx 1.46 \pm 0.06$ mag. SN 2005M is a spectroscopically peculiar object like SN 1991T. This supernova has a slower decline rate ($\Delta m_{15}(B) = 0.86 \pm 0.05$ mag), but it does not appear to be overluminous in either the UV or optical bands. However, our relative ignorance regarding the intrinsic color of these slow decliners might prevent us from deriving reliable reddenings for them. A notable feature in the plot is that the UV emission of SN 2004dt appears unusually strong around the *B*-band maximum and decreases rapidly after maximum light. Moreover, SN 2005M seems to peak a few days earlier than SN 2005cf in the F220W and F250W bands. Such a temporal shift seems to exist for SN 2004dt and SN 2004ef, although their light curves in UV are not well sampled around maximum brightness.

The color curves of our four SNe Ia, corrected for the MW and host-galaxy reddening, are presented in Figure 3. One can

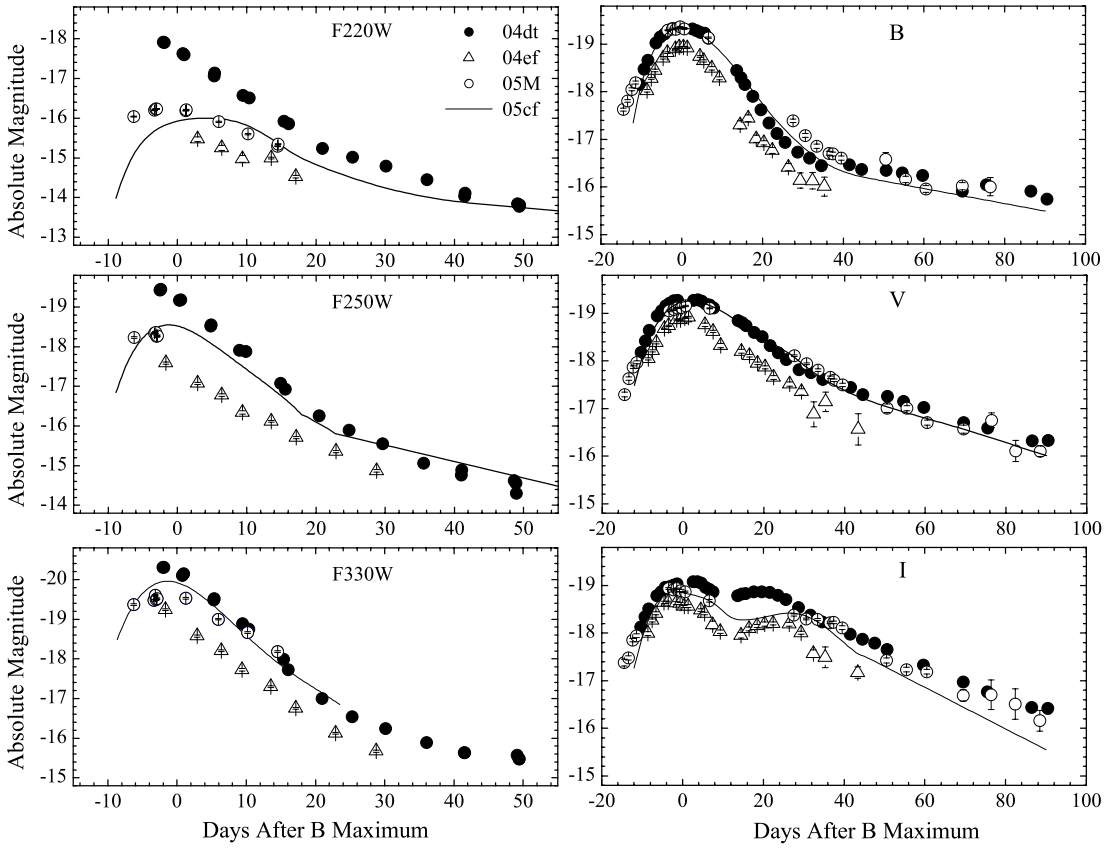

Figure 2. UV light curves of the Hubble-flow SNe 2004dt, 2004ef, and 2005M obtained with the *HST* ACS/HRC and the F220W, F250W, and F330W filters, together with the corresponding optical light curves in the *BVI* bands (Ganeshalingam et al. 2010). Overlaid are the UV–optical template light curves of the "gold standard" SN Ia 2005cf (W09b).

Table 3
Relevant Parameters for the *HST* UV Sample of Type Ia Supernovae

SN	Host Galaxy	$v_{3\,\mathrm{K},v220}$(km s^{-1})	μ (mag)	$\Delta m_{15}(B)$	$B_{\max} - V_{\max}$	$E(B-V)_{\mathrm{Gal}}$	$E(B-V)_{\mathrm{host}}$	Source
SN 2004dt	NGC 0799	5644	34.41(19)	1.13(04)	0.03(03)	0.020	0.08(04)	1, 2, 3
SN 2004ef	UGC 12158	8931	35.41(16)	1.46(06)	0.15(03)	0.056	0.11(05)	1, 3, 4
SN 2005M	NGC 2930	6891	34.81(17)	0.86(05)	−0.05(04)	0.022	0.10(05)	1, 3, 5
SN 2005cf	MCG-01-39-003	2143	32.31(34)	1.07(03)	0.09(03)	0.097	0.10(03)	6, 7

Notes. Uncertainty estimates in parentheses are in units of 0.01 mag.
References. (1) Ganeshalingam et al. 2010; (2) Altavilla et al. 2007; (3) Contreras et al. 2010; (4) Silverman et al. 2012; (5) Hicken et al. 2009; (6) Wang et al. 2009b; (7) Garavini et al. 2007.

clearly see that their UV$-V$ curves show remarkable differences despite having similar $B-V$ curves. SN 2004dt is quite peculiar, being very blue compared with the other three objects. It is worthwhile to point out that the *Swift* UVOT has seen a number of events (7) that are also blue in the NUV–optical photometric colors (P. Milne 2012, private communication).

Since SN 2004dt has $\Delta m_{15}(B) \approx 1.1$ mag and a peak $B-V$ color ($\sim$0.0 mag) similar to that of SN 2005cf, it is of interest to perform a detailed comparison of their UV properties. Around maximum light, SN 2004dt is bluer than SN 2005cf by $\sim$0.8 mag in F250W $-$ V and by $\sim$2.0 mag in F220W $-$ V. About 2–3 weeks after maximum, the color difference becomes less significant as a result of the rapid decline of the post-maximum UV emission in SN 2004dt (see Figure 6 and the discussion in Section 3.2). In the first 15 days after the maximum, the decline of the UV light curve is measured to be $\sim$1.9 mag in F220W, $\sim$2.4 mag in F250W, and $\sim$2.5 mag in F330W for SN 2004dt. These are all larger than the corresponding values measured for SN 2005cf by $\sim$0.6–0.9 mag (see also Table 10 in W09b). A faster post-maximum decline usually corresponds to a shorter rise time for the light curves of SNe Ia in the optical bands, as evidenced by the fact that they can be better normalized through the stretch factor (Perlmutter et al. 1997; Goldhaber et al. 2001). For SN 2004dt, a shorter rise time in the UV is consistent with the high expansion velocity that could make the gamma-ray heating less effective. Moreover, a higher expansion velocity could extend the radius of the UV photosphere to higher velocities and hence result in a larger UV flux. The possible origin of the UV excess in SN 2004dt in the early phase is an interesting issue and is further discussed in Section 4.2.

3.2. Ultraviolet Spectroscopy

As shown in Table 1, a total of 34 *HST* ACS PR200L prism spectra have been collected for SNe 2004dt, 2004ef, 2005M, and 2005cf. In Column 5 of Table 1, we list the total exposure time for each spectrum, resulting from a series of co-added

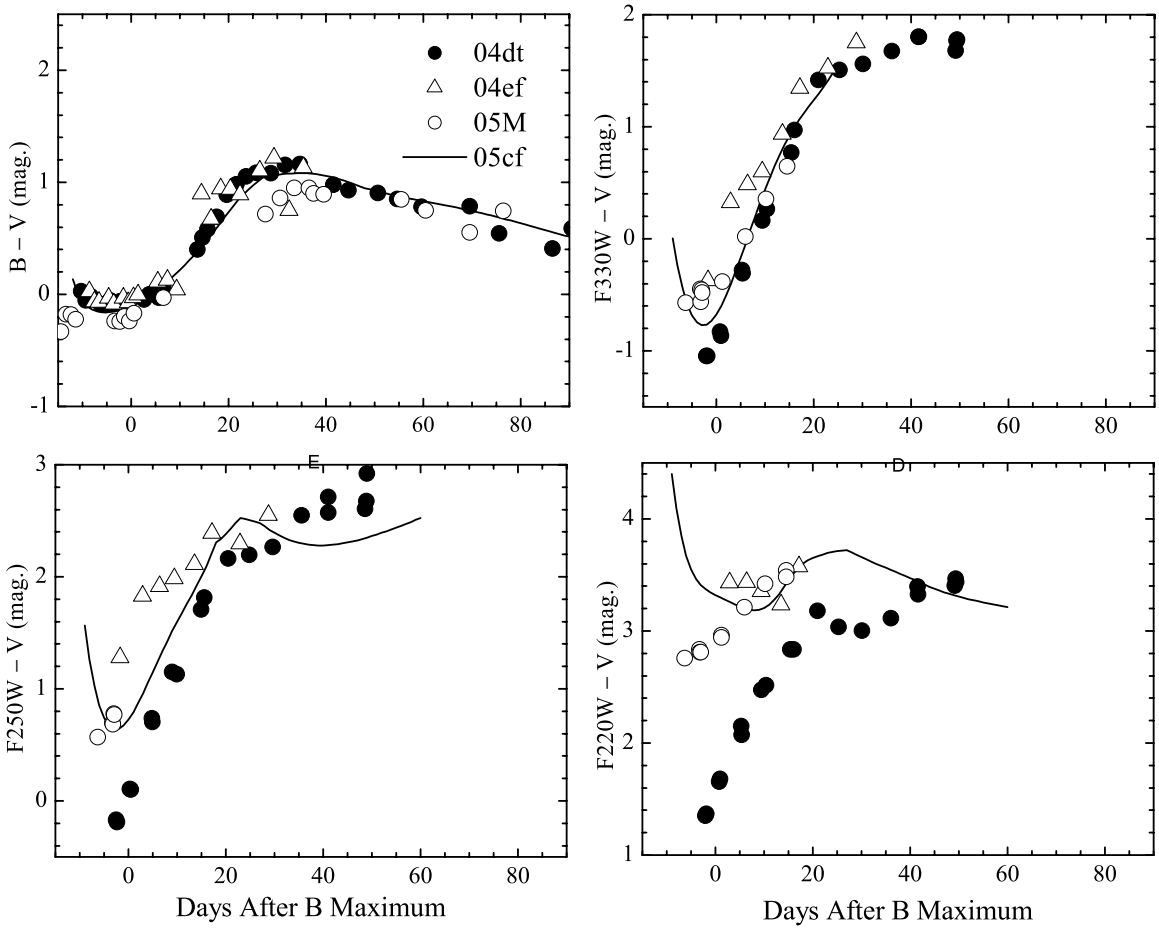

Figure 3. UV color curves of the Hubble-flow SNe 2004dt, 2004ef, and 2005M. Overlaid are the color-curve templates of the "gold standard" SN Ia 2005cf (W09b).

CR-split exposures. Among the four SNe Ia observed with the *HST* ACS, SN 2005cf and SN 2004dt have better temporal sequences and higher S/N for their UV spectra (see Figures 5 and 6). Owing to very low spectral resolution at longer wavelengths, our analysis in this paper is restricted to the useful wavelength range 1800–3500 Å.

To evaluate the quality of the prism data, we compare the synthetic magnitudes derived from the UV spectra with those obtained by direct imaging observations for SN 2005cf and SN 2004dt (see Figure 4). In F330W, these two measurements match well with each other near maximum light, but the spectrophotometric magnitudes decline more slowly starting about one week after maximum. A similar trend in the decline rate exists in the F220W and F250W bands of SN 2004dt and in the F250W band of SN 2005cf. However, compared with the corresponding imaging observations, it is alarming that the flux of the prism spectra is too high in the F250W band (∼0.6 mag for SN 2004dt, ∼0.7 mag for SN 2005cf), and especially in the F220W band (∼1.0 mag for SN 2004dt, ∼2.0 mag for SN 2005cf). This suggests that the flux level of PR200L calibrated by the white dwarfs (which are very blue) may not be accurate for the flux calibration of the supernova.

According to ACS/HRC Instrument science report ACS 2006-03 (Larsen et al. 2006), the flux calibration of the PR200L prism spectra based on white dwarfs is expected to be accurate to ∼5% over the wavelength range 1800–3000 Å. However, red objects usually suffer systematic errors in the UV flux calibration because the blue end of the spectrum can be highly contaminated by scattered light from the red end as a result of the "red pile-up" effect. Such an effect is probably a dominant factor accounting for the higher F250W and F220W fluxes, as indicated by the wavelength-dependent discrepancy between the spectrophotometry and observed photometry,[64] as well as for the slower post-maximum decline seen in all three UV bands for the SNe in our sample; SNe Ia are known to become progressively redder after maximum light, and the contamination of the red light becomes increasingly significant. However, the red pile-up effect is at present poorly quantified, and more test observations of objects covering a wide range of colors are clearly needed to better calibrate PR200L prism spectra.

Fortunately, we also have ACS HRC photometry taken nearly at the same time, making it possible to obtain accurate relative flux calibration of the PR200L prism spectra. Given the relatively smooth variations in the raw prism spectra, it is not difficult to model the continuum of the spectra with a simple polynomial function. The final calibrated spectra of SN 2005cf and SN 2004dt are shown in Figures 5 and 6; the spectrophotometry is consistent with the photometric results within ±0.05 mag. However, the observed increase in flux below about 2200 Å is almost certainly an artifact and should not be trusted.

The UV spectra of SN 2004ef have poor S/N; the object is relatively faint, being at a larger distance (∼120 Mpc). Only a single UV-prism spectrum was obtained of SN 2005M. The UV spectra of SN 2004ef and SN 2005M are shown in Figure 7.

[64] One can also see from Figure 1 that this effect is particularly obvious for SN 2005cf as a lot of photons have spilled over from the red to the blue of the dispersed image.

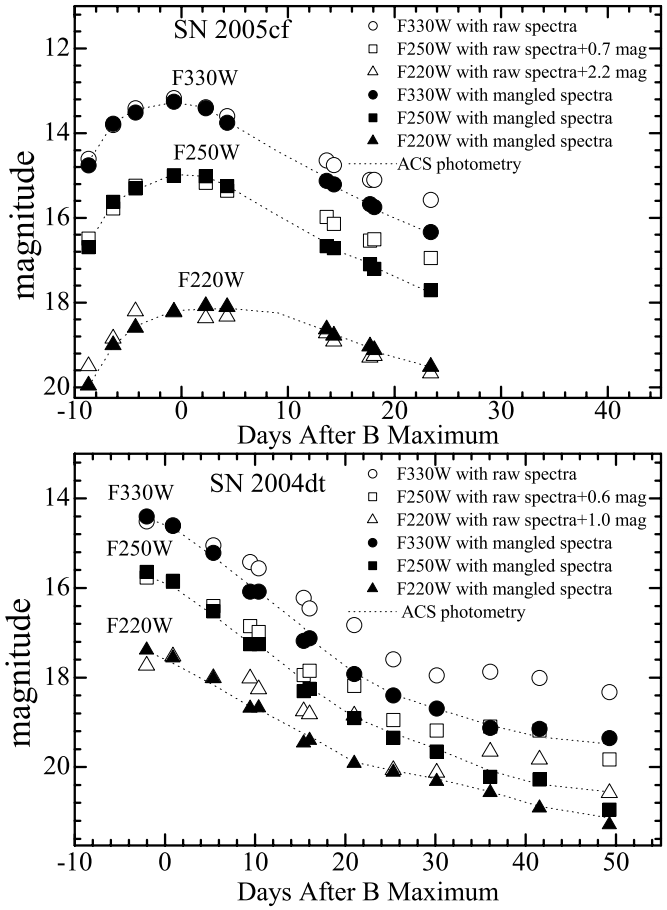

Figure 4. Comparison of the spectrophotometry with the observed photometry for SN 2004dt and SN 2005cf at UV wavelengths. The open symbols represent the synthetic magnitudes from the raw spectra, and the filled symbols represent the values from the spectra mangled to the observed photometry. The dashed curves represent the observed photometry.

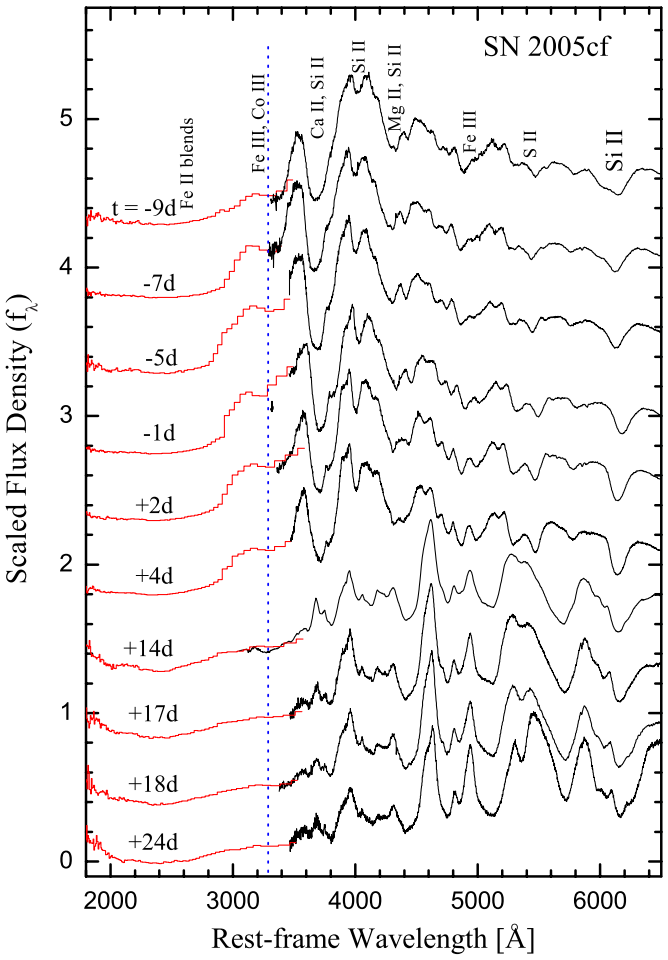

Figure 5. Evolution of the UV–optical spectrum of SN 2005cf. The UV spectra were obtained with the *HST* ACS prism (PR200L), and the corresponding optical data are taken from W09b and Garavini et al. (2007). All of the spectra have been rescaled to match the UV–optical photometry and were adjusted to the peak of the spectral flux and arbitrarily shifted for display. The dashed line marks the position of the ~3250 Å absorption feature. The increase in flux below about 2200 Å is almost certainly an artifact and should not be trusted.

(A color version of this figure is available in the online journal.)

3.2.1. SN 2005cf

Figure 5 shows the evolution of the combined UV–optical spectrum of SN 2005cf from $t = -9$ days to $t = +24$ days relative to the *B*-band maximum. The ground-based spectra are taken from W09a and Garavini et al. (2007). Spectra obtained within 1–2 days of each other were combined directly. In cases where no contemporaneous optical spectrum was available, an interpolated spectrum was used. After flux calibration with the corresponding ACS/HRC photometry, the UV-prism spectra agree reasonably well with their optical counterparts over the spectral range 3300–3500 Å (see Figure 5).

It is known that in the UV spectra of SNe Ia, almost no individual lines can be identified. This is because the vast number of iron-group element lines in the UV overlap strongly, eliminating individual line features. This contrasts with the optical, where P-Cygni lines of neutral or singly ionized ions of intermediate-mass elements (IMEs; mostly O, Mg, Si, S, and Ca) can usually be identified. Probably, the only individual feature in SN Ia UV spectra blueward of ~3700 Å that can be obviously identified is the P-Cygni line (absorption feature at ~2650 Å) caused by Mg II λ2800, which was seen in *HST* spectra of SN 1992A at $t = 5$ days after the *B* maximum (Kirshner et al. 1993). In our spectra, we see no clear evidence of this line or any other line-like feature blueward of ~2800 Å. In most of our spectra, this is probably caused by the low-S/N and low resolution. In the case of SN 2004dt, the effect that led to strong UV emission (e.g., circumstellar matter interaction) may have smoothed out line-like features (see the discussion below).

Inspecting the near-maximum UV spectra in the wavelength range 1800–3500 Å, we identify a prominent absorption feature near 3250 Å. It is also seen in the *Swift* UVOT UV-grism spectrum of SN 2005cf near maximum light (e.g., Bufano et al. 2009; see also Figure 9) and the STIS UV spectra of the Palomar Transient Factory sample of SNe Ia (Cooke et al. 2011). However, we note that the relatively weak absorption feature near ~3050 Å seen in STIS and *Swift* spectra is nearly invisible in the *HST* UV spectrum, indicating the limited resolution of the *HST*/ACS prism. The resolution effect can be demonstrated by degrading the *Swift* spectrum. The ~3050 Å feature becomes very weak in the *Swift* spectrum degraded to a resolution of ~50 Å pixel^{-1} (see the dash-dotted line in Figure 9), and this feature almost disappears when further decreasing the spectral resolution to ~100 Å pixel^{-1} (see the dashed line in Figure 9). The absorption feature near 3250 Å also becomes less significant at a resolution ~100 Å pixel^{-1}, consistent with that observed in the *HST* prism spectrum.

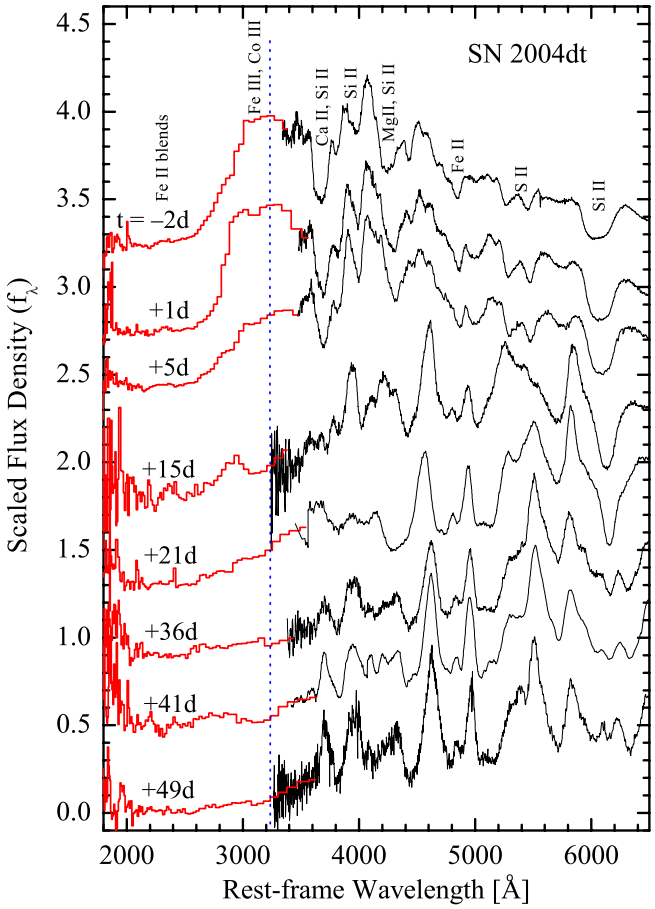

Figure 6. Evolution of the UV–optical spectrum of SN 2004dt. The UV spectra were obtained with the *HST* ACS/HRC PR200L prism, and the optical data are from Altavilla et al. (2007). All of the spectra have been rescaled to match the UV–optical photometry and were normalized to the flux peak of the spectrum and arbitrarily shifted for display. The vertical dashed line marks the position of the absorption feature near ∼3250 Å.

(A color version of this figure is available in the online journal.)

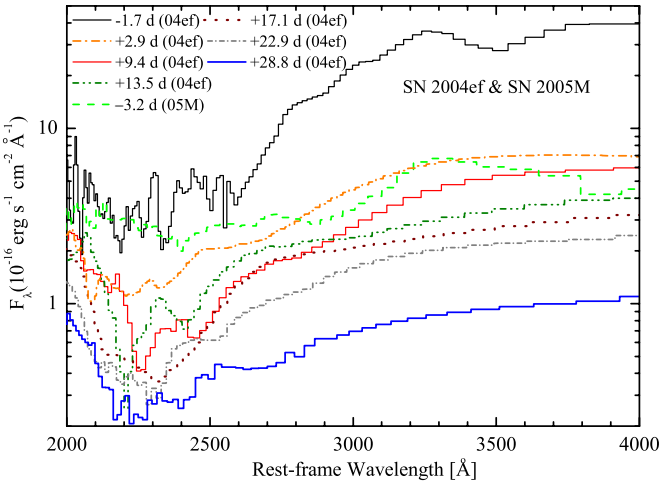

Figure 7. Evolution of the UV spectra of SN 2004ef and SN 2005M. The UV spectra were obtained with the *HST* ACS/HRC PR200L prism. The increase in flux below about 2200 Å is almost certainly an artifact and should not be trusted.

(A color version of this figure is available in the online journal.)

The flux ratio $R_{\rm UV}$, defined as $f_\lambda(2770\,\text{Å})/f_\lambda(2900\,\text{Å})$, has been proposed to correlate with the peak luminosity of SNe Ia (Foley et al. 2008). Our *HST* spectra are not appropriate for testing such a correlation due to their limited resolution ($\gtrsim$40 Å pixel^{-1} at 2800–2900 Å), which could have significant impact on the intrinsic UV slope within such a narrow wavelength range. Even more importantly, as discussed in Section 3.2, red pile-up affects the spectra substantially in this region.

The near-UV features in the ∼2700–3500 Å range of the early-time spectra of SNe Ia were initially studied by Branch & Venkatakrishna (1986), who suggested that they are produced by blends of Fe II and Co II lines. In particular, the ∼3250 Å absorption feature has been attributed to blueshifted Co II absorption (rest wavelength 3350–3500 Å; Branch et al. 1985), and the absorption feature at ∼3050 Å is ascribed to Fe II absorption. Based on their study of the prominent example SN 1992A, Kirshner et al. (1993) confirmed that the near-UV region is largely formed by a complex blend of iron-group element lines. They found that Cr II, Mn II, and Fe II contribute significantly to the absorption-like feature at ∼3250 Å, while the ions Co II and Ni II make no significant contribution because the newly synthesized Ni–Co is confined to the inner regions at these early phases. The spectral properties of SNe Ia in the UV were also investigated by Sauer et al. (2008), based on the early-time spectra of SN 2001eh and SN 2001ep obtained with *HST* STIS. In their study, the contributions of Ti II to the ∼3050 Å feature and of doubly ionized species such as Fe III and Co III to the ∼3250 Å features of SN 2001eh are important. The absorption features blueward of 2700 Å in the spectrum are also thought to originate from singly and doubly ionized Fe and Co (Kirshner et al. 1993; Sauer et al. 2008).

3.2.2. SN 2004dt

The evolution of the combined UV–optical spectrum of SN 2004dt is displayed in Figure 6. The UV spectroscopic observations of SN 2004dt cover the period from $t \approx -2$ days to $t \approx +50$ days with respect to the *B*-band maximum. The optical data shown in the plot are taken from Altavilla et al. (2007). At $t = -2$ days and $t = +1$ day, it is evident that there is a prominent peak emerging between 2900 Å and 3400 Å. The absorption-like feature at ∼3250 Å, as seen in SN 2005cf and other normal SNe Ia (Bufano et al. 2009, and this paper), is very weak and nearly invisible in SN 2004dt. This feature becomes prominent in the $t = +15$ day and $t = +41$ day spectra, but it is weak at other epochs after maximum brightness. This variation may be caused by the poor S/N, the lower resolution of the PR200L spectrum, possible errors in the data reduction, or a combination of the above factors. Moreover, the overall spectral flux in the UV region drops rapidly after maximum light, consistent with the rapid decline of the UV light curves (see Figure 2).

The strengthening of the ∼3200 Å feature in the post-maximum spectra is particularly interesting in the case of SN 2004dt. It may reflect an increase in the line-blanketing opacity as a result of a retreat of the photosphere into the iron-group-rich inner region of the ejecta, which is supported by the fact that the ∼5000 Å feature (due to blends of Fe II and Fe III) gradually gained strength after maximum brightness. The Doppler velocity of Si II λ6355 is found to be ∼14,000 km s^{-1} for SN 2004dt from the near-maximum spectrum, which fits comfortably in the high-velocity category (W09a). This object is also a member of the high-velocity-gradient group (Benetti et al. 2005) and the broad-line (BL) subclass (Branch et al. 2006). It is interesting to examine whether the distinct UV behavior correlates with the production of the high-velocity

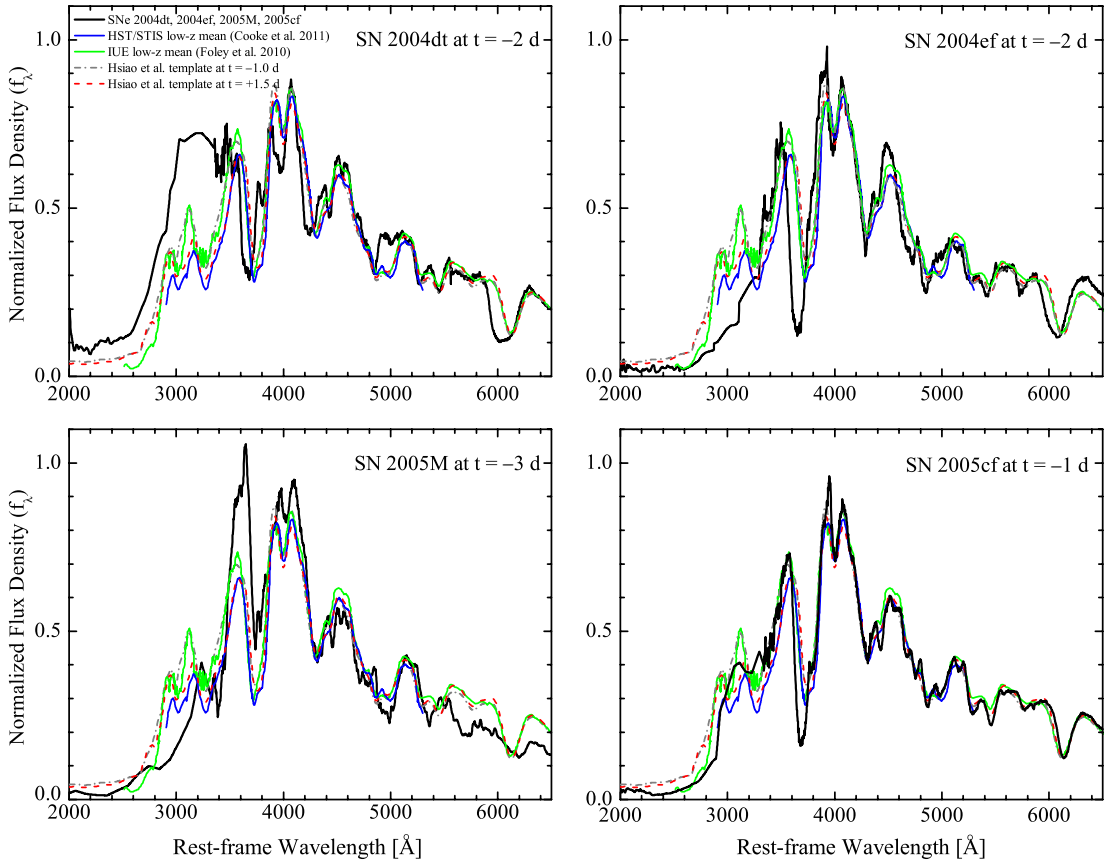

Figure 8. Comparison of the near-maximum-light UV–optical spectra of SNe 2004dt, 2004ef, 2005M, and 2005cf with the mean spectra of the low-redshift SNe Ia constructed by Cooke et al. (2011), Foley et al. (2012), and Hsiao et al. (2007). Note that the low resolution of our *HST* spectra may play a substantial role in affecting the spectral features below 3500 Å.

(A color version of this figure is available in the online journal.)

features in SNe Ia. The origin of the high-velocity features is still unclear. They could be due to an increase in the abundance and/or density in the outer layers, circumstellar material interaction (e.g., Gerardy et al. 2004; Mazzali et al. 2005), or a clumpy distribution of the outer ejecta (Leonard et al. 2005; Wang et al. 2006a).

3.2.3. SN 2004ef and SN 2005M

In Figure 7, we show the evolution of the UV spectrum of SN 2004ef, as well as a single-epoch spectrum of SN 2005M. The UV spectroscopic observations of SN 2004ef span from $t \approx -2$ days to $t \approx +29$ days with respect to the B-band maximum. A temporal sequence of the combined UV–optical spectra cannot be constructed for SN 2004ef due to the sparse optical data at similar phases.

As in SN 2005cf and SN 2004dt, the UV spectra of SN 2004ef show a broad and shallow absorption trough near 2300 Å, which is likely due to blending of the multiplets of the ionized iron-group elements (Kirshner et al. 1993). Note that the prominent absorption feature near 3250 Å, commonly seen in other SNe Ia, is invisible in the UV spectra of SNe 2004ef and 2005M. This inconsistency reminds us that the limited S/N and low resolution of the spectra could have significant influence on the observed features of the spectra.

3.2.4. Comparison of the UV Spectra

In Figure 8, we compare the near-maximum UV spectra of our four nearby SNe Ia with other mean low-redshift SN Ia spectra at similar phases. The spectra have been corrected for reddening in the MW. The mean low-redshift spectra come from several studies, including the mean spectrum constructed primarily with the *HST* STIS spectra (Cooke et al. 2011), the combined spectrum of a few nearby SNe Ia with archival *HST* and *IUE* data (Foley et al. 2012), and the spectral template established by Hsiao et al. (2007). As Cooke et al. (2011) did not apply any extinction correction in building their mean low-redshift spectrum, we apply a reddening correction to their spectrum, with $E(B-V) = 0.10$ mag and $R_V = 3.1$, to correct for the color difference. All of the spectra shown in the plot are normalized to approximately the same flux in the rest-frame wavelength range 4000–5500 Å. Note that the Hsiao et al. (2007) template spectra contain high-redshift SN Ia data from the Supernova Legacy Survey (Ellis et al. 2008); hence, they may suffer from evolutionary effects and may not represent the genuine spectrum of local SNe Ia in the UV region.

The Foley et al. spectrum (mean phase $t \approx 0.4$ days) and the Hsiao et al. $t = -1$ day spectrum agree fairly well within the uncertainties, and the STIS UV spectrum (mean phase $t \approx 1.5$ days) also shows reasonable agreement given the difference in epoch. We see that there is a general shift of UV peak features to the red between $t \approx -1$ day and $t \approx +1$ day. Most notably, the large peak near 3100 Å at $t \approx -1$ day shifts to ~3150 Å at $t \approx +1$ day. The underlying cause of the shift is probably just the recession in velocity of the UV photosphere with the expansion of the ejecta, but detailed modeling would be needed to verify this.

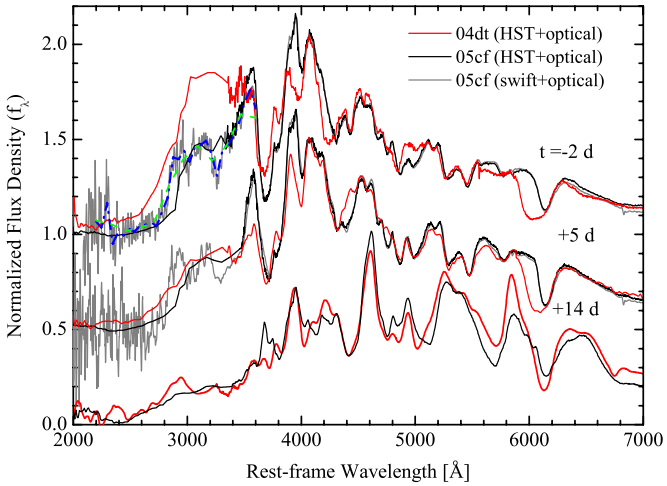

Figure 9. Comparison of the UV–optical spectra of SN 2004dt and SN 2005cf at three selected epochs ($t = -2$, +5, and +14 with respect to the B-band maximum). The dash-dotted (blue) and dashed (green) lines represent the *Swift* UV spectra of SN 2005cf degraded to a resolution of ∼50 Å and ∼100 Å, respectively.

(A color version of this figure is available in the online journal.)

Of our sample, SN 2004dt appears to be unusually bright in the UV. Its UV emission is found to be stronger than the Foley et al. low-redshift mean spectrum for $t \approx -1$ day by $\gtrsim$75% (or at a confidence level $\gtrsim 6\sigma$–7σ) at wavelengths 2500–3500 Å. Differences are also present in the optical portion of the spectrum where the absorption features of IMEs are relatively strong and highly blueshifted (except for the S II lines), although the integrated flux over this region does not show significant differences with respect to the templates. The ∼5000 Å absorption feature due to Fe II and Fe III blends appears to be rather weak, perhaps suggestive of a smaller amount of iron-peak elements in the outer ejecta of SN 2004dt.

The near-maximum spectrum of SN 2004ef displays prominent features of both IMEs and Fe-group elements, with the UV emission being weaker than the local composite spectrum by about 25%. Another notable aspect of Figure 8 is the deficiency of the UV emission in SN 2005M. This supernova exhibits the prominent Fe III feature near 5000 Å in the earliest spectrum (Thomas 2005). SN 2005M has a smaller $\Delta m_{15}(B)$; however, the UV flux emitted in the wavelength region 2500–3500 Å is found to be even lower than the mean value by ∼22%. One can see from Figure 8 that significant scatter is observed in these three events at wavelengths below ∼3500 Å. In this wavelength region, the continuum and the spectral features were proposed to be primarily shaped by heavy elements such as Fe and Co (Pauldrach et al. 1996). Thus, the large scatter in our sample might be related to variations of the abundance of Fe and Co in the outer layers of the exploding white dwarf (Höflich et al. 1998; Lentz et al. 2000; Sauer et al. 2008). On the other hand, the spectrum of SN 2005cf generally matches well the nearby comparison except for the Ca II H&K feature, which exhibits the strongest difference in the optical region among our four events. The variations of Ca II and Si II absorptions at higher velocities suggest that additional factors, such as asphericity or different abundances in the progenitor white dwarf, affect the outermost layers (Tanaka et al. 2008).

Figure 9 shows a more detailed comparison of the UV–optical spectra of SN 2004dt and SN 2005cf at three different epochs ($t \approx -2$ days, +5 days, and +14 days). The integrated fluxes of the spectra have been normalized over the 4000–5500 Å wavelength range. These two SNe Ia provide us good examples to examine the generic scatter in the UV region as they have quite similar photometric properties in the optical bands, such as the $B - V$ color at maximum and the post-maximum decline rate $\Delta m_{15}(B)$ (see Table 3). At $t \approx -2$ days, the normalized flux obtained for SN 2004dt at 2500–3500 Å is much brighter than for SN 2005cf in the same wavelength region, with the flux ratio $F_{04dt}/F_{05cf} \approx 1.9$. This flux ratio in the UV decreases quickly to ∼1.2 at $t \approx +5$ days, and it becomes roughly 1.0 at $t \approx 2$ weeks after maximum. Neither contamination by the background light from the host galaxy nor uncertainty in the reddening correction is likely to account for such a peculiar evolution of the UV flux for SN 2004dt; the influence of background emission would become more prominent as the object dims and SN 2004dt does not suffer significant reddening in the host galaxy (see Section 4). Such a fast decline of the UV flux is rarely seen in the existing sample of SNe Ia, possibly an indication of differences in the explosion physics or progenitor environment with respect to normal SNe Ia.

3.3. General Properties of the UV Luminosity of SNe Ia

The peak luminosity of SNe Ia in the optical bands has been extensively studied and found to correlate well with the width of the light curve around maximum light. Outliers have been identified as abnormal objects with different explosion mechanisms such as the overluminous objects SN 2003fk (Howell et al. 2006) and SN 2009dc (Silverman et al. 2011; Taubenberger et al. 2011) and the underluminous events SN 1991bg (Filippenko et al. 1992a; Leibundgut et al. 1993) and SN 2002cx (Li et al. 2003). Examining the relationship between the UV luminosity and $\Delta m_{15}(B)$ may disclose a diversity, even for the so-called normal SNe Ia, since the UV emission is thought to be more sensitive to possible variations of the explosion physics or progenitor environment.

We have examined a sample of 20 SNe Ia with good photometry in the UV. Four among this sample are from the *HST* observations presented in this paper, and the rest are *Swift* objects published by Milne et al. (2010). The left panels of Figure 10 show the maximum absolute magnitudes of these objects in broadband U, B, and *Swift* uvw1/*HST* F250W versus $\Delta m_{15}(B)$.[65] Following the analysis by Brown et al. (2010), we applied the red-tail corrections to the uvw1/F250W magnitudes to mitigate the effects of the optical photons on the UV flux. The U and uvw1/F250W magnitudes are also K-corrected for the large variation in the spectral flux at shorter wavelengths (but note that a UV/blue event like SN 2004dt may warrant a second spectral sequence for the sake of red-tail and K-corrections). The peak magnitudes in the uvw1/F250W filters are obtained by fitting the data with a polynomial or the template light curve of SN 2005cf. The parameters in the optical bands, such as the peak magnitudes and the B-band light-curve decline rate $\Delta m_{15}(B)$, are estimated from the published light curves (see Table 3 and the references).

After corrections for the extinction (assuming an extinction law with $R_V = 2.3$ for the SN host galaxy), linear fits to the subsample in Figure 10 with 0.8 mag $< \Delta m_{15}(B) <$ 1.7 mag

[65] As the instrumental response curve of the *HST* ACS F250W filter is similar to that of the *Swift* uvw1, the magnitudes measured in these two filters should be comparable. This is demonstrated by the observations of SN 2005cf, for which the measurements by the *HST* ACS and the *Swift* UVOT are consistent to within 0.1 mag (W09b). We thus neglect magnitude differences measured in the F250W and the uvw1 filters in our analysis.

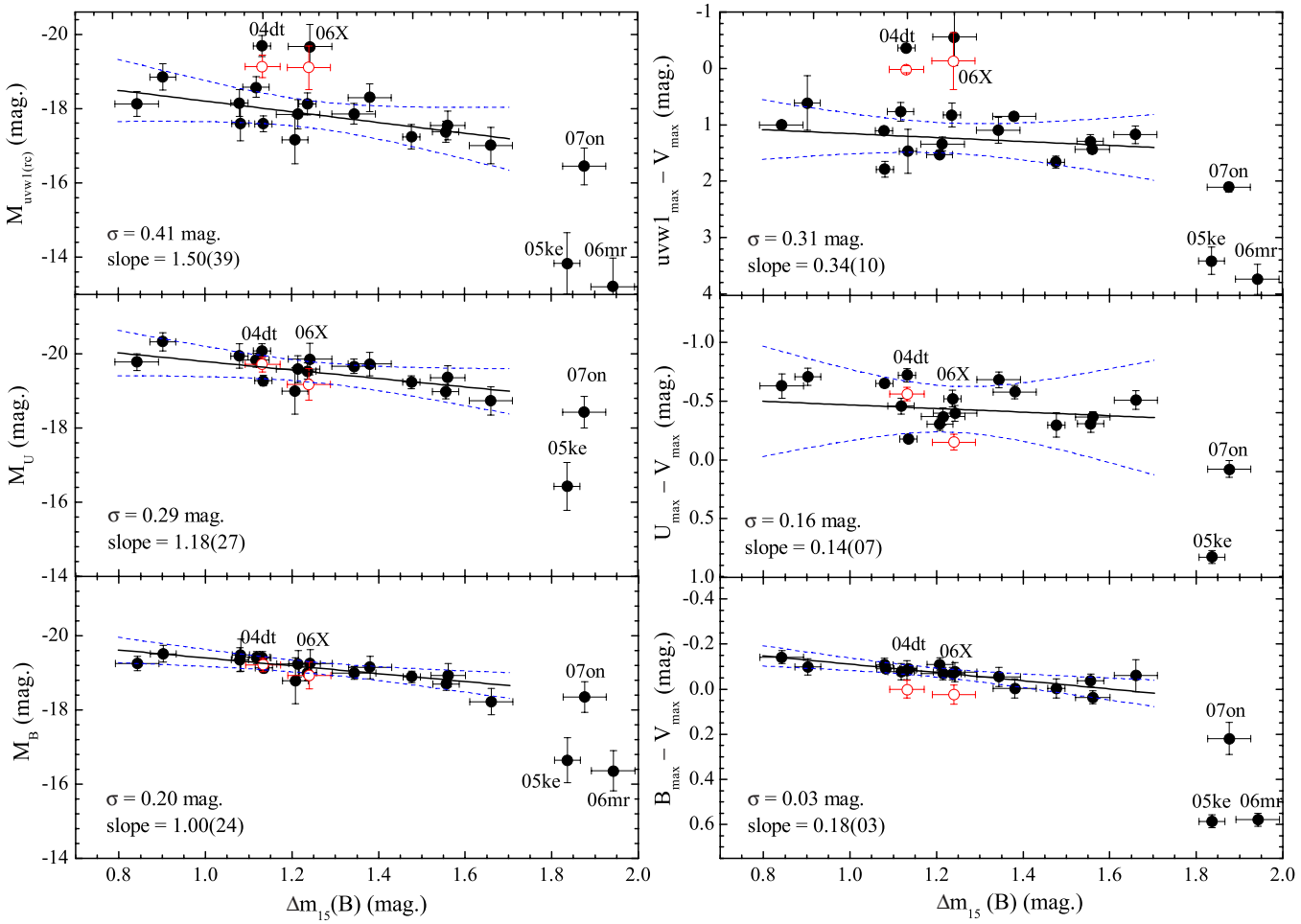

Figure 10. Left panels: the uvw1-, *U*-, and *B*-band maximum magnitudes vs. the *B*-band decline-rate parameter $\Delta m_{15}(B)$ of SNe Ia with UV observations from the *Swift* UVOT and *HST*. Right panels: the peak colors plotted vs. $\Delta m_{15}(B)$. The solid lines represent the linear fit to the SNe with 0.8 mag $< \Delta m_{15}(B) <$ 1.7 mag, and the dashed curves represent the 3σ uncertainties. SN 2004dt and SN 2006X are not included in the fit, while the open symbols show the case assuming that these two SNe Ia have intrinsically redder color by ∼0.1 mag with respect to the other objects.

(A color version of this figure is available in the online journal.)

yield a root-mean-square scatter (i.e., σ values) of ∼0.2 mag in *B* and ∼0.4 mag in uvw1. Note that SN 2004dt and SN 2006X were excluded from the fit. The uvw1-band peak luminosity does show a correlation with $\Delta m_{15}(B)$, but with steeper slopes and larger scatter than that in *B* and *U*. Given the fact that the dust obscuring the SN may have different origins (e.g., Wang 2005; Goobar 2008; W09a), the host-galaxy extinction corrections with $R_V = 3.1$ (MW dust) and $R_V = 1.8$ (LMC dust) are also applied to the absolute magnitudes. In both cases, the scatter also increases at shorter wavelengths. The relevant results of the best linear fit with different values of R_V to the $M_{\rm max}$–$\Delta m_{15}(B)$ relation are shown in Table 4.

The wavelength-dependent scatter can be driven in part by the uncertainty in the absorption corrections, as the UV photons are more scattered by the dust than the optical. Assuming a mean error ∼0.04 mag in $E(B-V)_{\rm host}$ (e.g., Phillips et al. 1999; Wang et al. 2006a), the residual scatter of the uvw1-band luminosity can be as large as ∼0.3 mag, which is still much larger than that found in *B* (∼0.15 mag). A notable feature in the left panel of Figure 10 is the UV excess seen in SN 2004dt and perhaps SN 2006X; they are found to be brighter than the corresponding mean value by $\sim 6.0\sigma$ and $\sim 3.0\sigma$, respectively. The discrepancy of the observed scatter cannot be caused by the error in distance modulus, which applies equally to the UV and optical bands. This is demonstrated by the correlation between the peak colors and $\Delta m_{15}(B)$, as shown in the right panels of Figure 10. The color correlation is distance independent, but it shows significantly large scatter in the UV. In particular, the

Table 4
Linear Fit to the $M_{\rm max}$–$\Delta m_{15}(B)$ Relation $M_{\rm max} = M_0 + \alpha(\Delta m_{15}(B) - 1.1)$

Bandpass	M_0 (mag)	α	Number	σ (mag)
		$R_{{\rm MW},V} = 3.1$		
uvw1	−18.18(10)	−1.58(39)	15	0.44
U	−19.88(07)	−1.47(27)	14	0.35
B	−19.42(07)	−1.27(24)	14	0.23
		$R_V = 2.3$		
uvw1	−18.12(10)	−1.50(39)	15	0.41
U	−19.67(07)	−1.18(27)	14	0.29
B	−19.23(07)	−1.00(24)	15	0.20
		$R_{{\rm CSLMC},V} = 1.8$		
uvw1	−18.05(10)	−1.38(39)	14	0.40
U	−19.60(07)	−1.08(27)	14	0.28
B	−19.24(07)	−1.01(24)	14	0.20

Note. Uncertainty estimates in parentheses are in units of 0.01 mag.

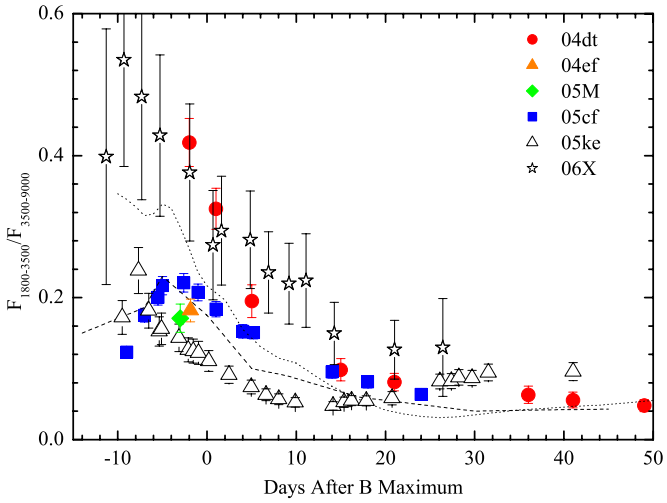

Figure 11. Flux ratio of the UV (1800–3500 Å) portion to the optical flux (3500–9000 Å), measured from the flux-calibrated UV–optical spectra of SNe 2004dt, 2004ef, 2005M, 2005cf, 2005ke, and 2006X (see the text for the sources of the data). The dotted line is the flux ratio computed from the template spectra from Hsiao et al. (2007); the dashed curve is the flux ratio estimated from a few nearby SNe Ia with the UV observations (Stanishev et al. 2007).

(A color version of this figure is available in the online journal.)

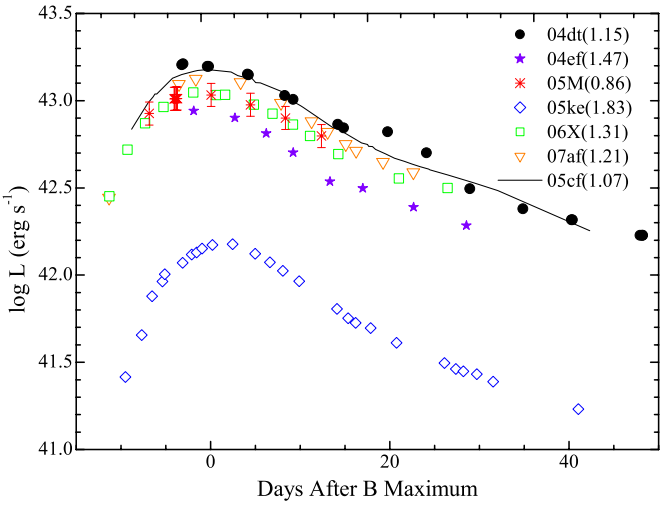

Figure 12. UV/optical/IR quasi-bolometric light curves of SNe 2004dt, 2004ef, 2005M, and 2005cf. Overplotted are the corresponding light curves of the comparison SNe Ia. The numbers in parentheses represent the $\Delta m_{15}(B)$ values for the SNe Ia.

(A color version of this figure is available in the online journal.)

uvw1/F250W$-V$ colors of SN 2004dt and SN 2006X are found to be bluer than the mean value by ∼1.3 mag. This indicates that the uvw1/F250W filter is perhaps more a probe of SN Ia physics than a cosmological standard candle.

Strong emission in the UV is likely an intrinsic property of SN 2004dt rather than being due to improper corrections for the dust reddening, since we only applied a small reddening correction to this supernova, $E(B-V)_{\rm host} = 0.08$ mag. Moreover, SN 2004dt still appears much brighter and bluer in the UV than the mean values defined by the other SNe Ia even if it is assumed to suffer little reddening. On the other hand, SN 2006X is heavily extinguished by dust having an abnormal extinction law, perhaps with $R_V \approx 1.5$ (Wang et al. 2008a). Applying this extinction correction (which is an extrapolation from the results of Wang et al. 2008a) and the red-tail correction (which is an extrapolation from the results of Brown et al. 2010) to the UV magnitudes of SN 2006X would make it appear brighter than the other comparisons by $\sim 1.7 \pm 0.6$ mag in uvw1/F250W. We caution, however, that this result may suffer large uncertainties from the speculated extinction and red-tail corrections.

4. DISCUSSION

4.1. Bolometric Light Curve and Nickel Mass

To examine how the relative flux in the UV evolves after the SN explosion, we compute the ratio of the UV emission (1800–3500 Å) to the optical (3500–9000 Å), $F_{\rm UV}/F_{\rm opt}$, for a few SNe Ia, as shown in Figure 11. The flux ratios obtained for SN 2005cf and SN 2005ke are overplotted. The dotted curve represents the Hsiao et al. (2007) template, and the dashed curve shows a combined template of SNe 1981B, 1989B, 1990N, 1992A, and 2001el (Stanishev et al. 2007). The flux ratios were calculated by integrating the flux-calibrated, UV–optical spectra except for SN 2005ke and SN 2006X. The integrated fluxes of these two SNe Ia are obtained approximately by the mean flux multiplied by the effective width of the passband. It is noteworthy that the flux ratio shown for SN 2006X might be just a lower limit, as we did not include the flux contribution below 2500 Å in the analysis because of the larger uncertainties in the extinction, K-corrections, and red-tail corrections at shorter wavelengths (e.g., Brown et al. 2010).

We note that the $F_{\rm UV}/F_{\rm opt}$ value of SN 2006X peaks at $t \approx 10$ days before the B-band maximum, about 5 days earlier than for SN 2005cf and the templates. This feature is similarly observed in the fast-decliner SN 2005ke, which exhibited a possible signature of X-ray emission as well as evidence for a UV excess in the early nebular phase, perhaps suggestive of circumstellar interaction (Immler et al. 2006). Owing to the lack of earlier UV data, we cannot conclude whether such a feature is present in SN 2004dt. It is apparent that the flux ratio $F_{\rm UV}/F_{\rm opt}$ exhibits a large scatter at comparable phases for the selected sample of SNe Ia. Consequently, the spread in bolometric corrections may affect significantly the inferring of the nickel masses from the light-curve peaks.

The overall properties of the SNe can be represented by their quasi-bolometric (UV/optical/IR) light curves shown in Figure 12. The near-infrared (NIR) photometry of SNe 2004ef and 2005M was taken from Contreras et al. (2010). The NIR emission of SN 2004dt was corrected on the basis of SN 2005cf (W09b). Similar corrections were applied to the comparison SNe Ia when the NIR observations were not available. Overall, the quasi-bolometric light curves of our SNe Ia are very similar in shape, with the exception of SN 2004dt, which shows a prominent "bump" feature. This "bump" is consistent with the secondary maximum visible in the I band (see Figure 2), being more prominent and occurring 10 days earlier than that of the other comparisons. This observed behavior suggests that SN 2004dt may have a larger, cooler iron core, or a higher progenitor metallicity according to the study of the physical relation between a supernova's NIR luminosity and its ionization state (Kasen 2006).

The bolometric luminosity at maximum light of SN 2004dt is estimated to be $L_{\rm max} \approx (1.7 \pm 0.2) \times 10^{43}$ erg s^{-1} with $R_V = 2.3$ and $E(B-V)_{\rm host} = 0.08$ mag. This value is consistent with that obtained for SNe Ia with similar Δm_{15} such as SN 2005cf [$\sim (1.5 \pm 0.2) \times 10^{43}$ erg s^{-1}] and SN 2007af [$\sim (1.3 \pm 0.2) \times 10^{43}$ erg s^{-1}] within 1σ–2σ errors. With the derived peak luminosity, we can estimate the ^{56}Ni mass ejected during the

explosion (Arnett 1982). According to Stritzinger & Leibundgut (2005), the ^{56}Ni mass ($M_{\rm Ni}$) can be written as a function of the bolometric luminosity at maximum and the rise time t_r:

$$L_{\rm max} = \left(6.45e^{-t_r/(8.8\,{\rm days})} + 1.45e^{-t_r/(111.3\,{\rm days})}\right) \times \left(\frac{M_{\rm Ni}}{M_\odot}\right) \times 10^{43}\,{\rm erg\ s^{-1}}. \quad (1)$$

Taking the rise time t_r as ~20 days for SN 2004dt and SN 2005cf, ~18 days for SN 2004ef, and ~24 days for SN 2005M (e.g., Ganeshalingam et al. 2011), the corresponding mass of the ejected ^{56}Ni is roughly estimated to be $0.9 \pm 0.1\,M_\odot$, $0.8 \pm 0.1\,M_\odot$, $0.4 \pm 0.1\,M_\odot$, and $0.7 \pm 0.1\,M_\odot$, respectively.

We see that the deduced $M_{\rm Ni}$ of the four SNe Ia shows significant scatter, and the value for SN 2004dt is slightly larger than the normal values. The net effect of a larger $M_{\rm Ni}$ would tend to delay the secondary maximum of the NIR light curves, inconsistent with what is seen in SN 2004dt. This inconsistency can be resolved if SN 2004dt has a shorter rise time, $t_r \approx 18.0$ days. Given the observational evidence that longer t_r usually corresponds to slower post-maximum decline of the light curve (Ganeshalingam et al. 2011), SN 2004dt may rise to maximum at a faster pace. A shorter rise time is likely to be a common feature of the high-velocity SNe Ia (Zhang et al. 2010; Ganeshalingam et al. 2011). Therefore, the deduced nickel mass of SN 2004dt may have been overestimated to some extent. On the other hand, the implied $M_{\rm Ni}$ for SN 2005M seems quite normal and is lower than in slowly declining SNe Ia such as SN 1991T, indicating that the light-curve widths are not a single-parameter family of the ejected nickel mass.

4.2. Origin of the UV Excess in SN 2004dt

The UV emission of SNe Ia is thought to originate predominantly from the outer layers of the ejecta because UV photons produced in deeper layers are subject to line blanketing by the wealth of bound–bound transitions associated with iron-group elements. Therefore, UV features are a promising probe to study the composition of the outer ejecta of SNe Ia.

Previous work has shown that the UV is particularly sensitive to the metal content of the outer ejecta (line-blocking effect) and their ionization (backwarming effect; Lentz et al. 2000; Sauer et al. 2008). Lentz et al. (2000) suggested a correlation between the emitted UV flux and the progenitor metallicity, with lower flux for models with higher metallicity. On the other hand, Sauer et al. (2008) proposed that the UV flux can become stronger at high metallicity in the outer layers due to an enhanced reverse-fluorescence scattering of photons from red to blue wavelengths and a change in the ionization fraction (backwarming effect). According to the model series for SN 2001eh and SN 2001ep (Sauer et al. 2008), as well as the prediction by Lentz et al. (2000), an abundance change of about ±2.0 dex (e.g., variations from 1/10 normal metallicity in the C+O layer to 10 times normal metallicity in the C+O layer) could lead to a change of up to ~0.3 mag in F250W/uvw1. This is much smaller than that observed in SN 2004dt. Note that the above studies are based on the one-dimensional deflagration model W7 (Nomoto et al. 1984).

To illustrate the effect of different progenitor metallicity on the UV spectra in more detail, we also consider a sub-Chandrasekhar-mass detonation model proposed by Sim et al. (2010). In particular, we adopt the model of a 1.06 $M_\odot$ CO white dwarf (model 1.06), which was found to give good agreement with the observed properties of normal SNe Ia in the optical. For this model, Sim et al. (2010) studied the effect of progenitor metallicity on the nucleosynthetic yields and, in turn, the synthetic observables. For that purpose they polluted the initial CO white dwarf with 7.5% ^{22}Ne (corresponding to a progenitor metallicity of ~3 $Z_\odot$). From this they find that the metallicity mainly affects the blue bands (specifically, they find the B-band peak magnitude to be ~0.5 mag dimmer for the model with $Z = 3\,Z_\odot$ compared to the model with $Z = 0$). In Figure 13(a), we show the UV spectra of these models at maximum light, which were obtained using Monte Carlo radiative transfer code ARTIS (Kromer & Sim 2009). To get better coverage in progenitor metallicity, we added another model at $Z = Z_\odot$ that was obtained in exactly the same manner as described by Sim et al. (2010). It is clearly seen that the UV flux increases significantly with decreasing progenitor metallicity. However, comparing the synthetic spectra to observed spectra of SN 2004dt, it is also obvious that the metallicity effect cannot be the dominant factor responsible for the unusual brightness of SN 2004dt in the UV, as it is not possible to enhance the UV flux farther than for the model with zero metallicity.

SN 2004dt shows line-expansion velocities which are apparently larger than those of normal SNe Ia. To investigate if these higher ejecta velocities can explain the UV excess of SN 2004dt, we adopted the standard deflagration model W7 (Nomoto et al. 1984), which is known to reproduce the observed maximum-light spectra of SNe Ia very well. The $t \approx 0$ day models shown in Figure 13(b) were calculated using the time-dependent PHOENIX code in local thermodynamic equilibrium (Jack et al. 2009, 2011). The velocities in W7 were increased by a uniform factor (20% or 40%). The densities were adjusted so that the total mass was conserved. Figure 13(b) clearly shows enhanced UV emission when the velocities are larger; the effects of line blending in the UV serve to increase the radius of the UV pseudophotosphere. Normalizing the spectral flux over the 4000–5500 Å region, we find that the UV flux emitted in the 2500–3500 Å region can be increased by about 40% if the expansion velocity $v_{\rm exp}$ is increased by 20% everywhere in W7. Note that increasing $v_{\rm exp}$ by 40% does not further enhance the UV flux, and the resulting flux increase in the 2500–3500 Å region drops to 34%. This indicates that an increase of the expansion velocity can lead to more UV flux, but it cannot reproduce the very large flux enhancement near 3000 Å in SN 2004dt.

Interestingly, SN 2004dt is the most highly polarized SN Ia ever observed. Across the Si II line its polarization $P_{\rm Si\,II}$ reaches up to 1.6% at ~1 week before maximum light (Wang et al. 2006a), indicating that its Si II layers substantially depart from spherical symmetry. Among the comparison sample, SN 2006X also has a large degree of polarization in the early phase, with $P_{\rm Si\,II} \approx 1.1\%$ at 6 days before maximum light (Patat et al. 2009). Thus, it could well be that viewing-angle effects play a major role in the observed UV excess of SN 2004dt. Breaking of spherical symmetry in the explosion is also thought to be a critical factor responsible for the observed scatter among SNe Ia (e.g., Wang et al. 2007; Kasen et al. 2009; Maeda et al. 2010; Maund et al. 2010).

Kromer & Sim (2009) recently studied the effect of asymmetric ejecta on the light curves and spectra of SNe Ia using an ellipsoidal (prolate) toy model. They found that SNe observed along the equator-on axis are always brighter than those observed along the pole-on axis. This effect is strongest in the bluer bands because the photons at short wavelengths are more strongly trapped than photons in other bands and therefore tend to preferentially leak out along the equatorial plane where the

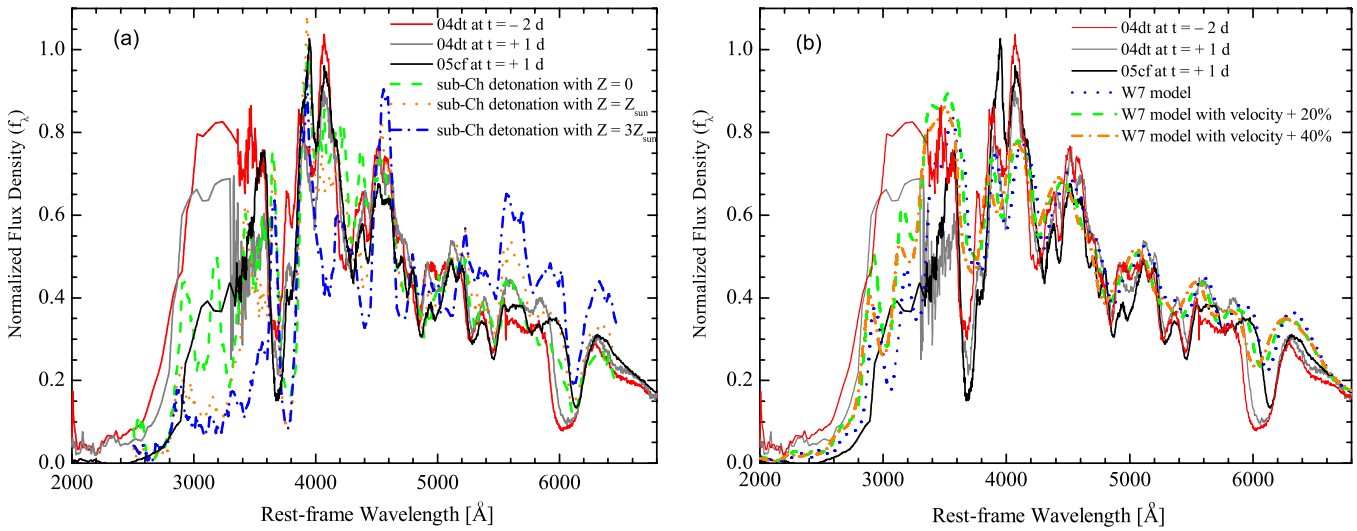

Figure 13. Left panel: comparison of the UV spectra of SN 2004dt near maximum light with synthetic UV spectra produced at a comparable phase by the sub-Chandrasekhar detonation model with different metallicity. Right panel: similar comparison with the synthetic spectra, but obtained with the W7 model and different expansion velocities.

(A color version of this figure is available in the online journal.)

photospheric velocity is smallest. Around maximum light, the difference $\Delta M = M_{\rm pole} - M_{\rm equator}$ measured in the U band could be ∼0.4 mag larger than that in the V band (Kromer & Sim 2009). After maximum light, this line-of-sight effect becomes weaker with time as the ejecta become optically thin at these wavelengths. Thus, the UV excess seen in SN 2004dt could also be due to a geometric effect.

We have described how there are several competing possible explanations for the enhanced UV flux in SN 2004dt. This is due to the complex nature of line blanketing in the barely optically thick, but highly scattering dominated, differentially expanding SN Ia atmosphere. This effect was described in part by Bongard et al. (2008), who showed that the complete spectrum is formed throughout the semitransparent atmosphere and that Fe III lines produce features that are imprinted on the full spectrum, partially explaining the UV excess found in SN 2004dt. Indeed, the differing results of Höflich et al. (1998) and Sauer et al. (2008), compared with those of Lentz et al. (2000), are perhaps due to the complex nature of spectral formation, ionization, and radiative transfer effects.

While asymmetry could play some role, there seems to be enough variation in spherically symmetric models due to effects of varying ionization that is likely produced by a density profile that differs from that of W7. Recall that W7 has a density bump that occurs when the flame is quenched and momentum conservation causes material to pile up ahead of the dying flame. Also, the higher brightness and indications of a somewhat higher nickel mass in SN 2004dt will affect the ionization state of the iron-peak elements, which are almost certainly responsible in part for the observed UV excess. More UV observations of nearby SNe Ia are needed to thoroughly understand these effects, and whether they are due to asymmetries or other phenomena in the explosion.

5. CONCLUSIONS

We have presented *HST* ACS UV photometry and spectra of SNe Ia obtained during Cycle 13 (2004–2005). These data include 34 ACS prism spectra and 110 photometric observations of four SNe Ia (SNe 2004dt, 2004ef, 2005M, and 2005cf). The spectral analysis is limited by the low resolution and low S/N of the data. However, comparison with the existing low-redshift mean spectra of SNe Ia clearly indicates that significant dispersion exists at wavelengths below ∼3500 Å. In particular, SN 2004dt is found to show a prominent, broad emission peak at 3000–3500 Å in the near-maximum spectrum, rather than having an absorption-like feature at ∼3250 Å similar to that in normal SNe Ia such as SN 2005cf. Another interesting feature of SN 2004dt is the rapid decline of its UV emission after the peak.

Based on a larger sample of SNe Ia, we studied the properties of their peak luminosity in the UV region. The luminosity in uvw1/F250W shows a correlation with the light-curve parameter $\Delta m_{15}(B)$, but with significantly larger scatter than that found in the optical: ∼0.4 mag in uvw1/F250W versus ∼0.2 mag in B. The increased dispersion in the UV has also been noted in other studies with independent SN Ia samples of both photometry (e.g., Guy et al. 2007; Brown et al. 2010) and spectra (Ellis et al. 2008; Cooke et al. 2011; Foley et al. 2012), which is likely intrinsic and has been interpreted as compositional differences between events. However, variations of the abundance based on either the W7 model or the sub-Chandrasekhar-mass detonation model cannot account for the UV excess seen in SN 2004dt. The W7 model with increased expansion velocities has also been investigated, but it can explain only part of the large UV flux in this object.

In our study, the comparison object SN 2006X may also exhibit strong emission in the UV. Some common features for SN 2004dt and SN 2006X are the distinctly high-velocity features beyond the photosphere, slower B-band light-curve evolution in the early nebular phase (Wang et al. 2008a), and a large degree of ejecta polarization near the optical maximum (Patat et al. 2009). The above-observed features of these two objects are perhaps related to an asymmetric explosion of the high-velocity SNe Ia (X. Wang et al. 2012, in preparation). Line-of-sight effects due to the asymmetric explosion can have a more significant effect on the observed scatter in the UV than in other bands. A new proposal to identify the progenitors based on the symmetry properties of the explosion has recently been proposed by Livio & Pringle (2011). However, more detailed

studies are clearly needed to investigate this fully for realistic models.

The question of whether a UV excess is a more general property of the high-velocity subclass merits further study with a larger sample having earlier observations like PTF 11kly/SN 2011fe (Brown et al. 2011). We note, however, that the origin of the high-velocity features and large polarization observed in SN 2004dt and SN 2006X probably differs, since the former does not follow the relation between the early-phase velocity gradient and the nebular-phase emission-line velocity shift while the latter does (Maeda et al. 2010). SN 2004dt is also found to be an outlier in the relation between the line polarization of Si II λ6355 and the nebular velocity offset (Maund et al. 2010). Moreover, the reddening of SN 2004dt by its host galaxy is low, while SN 2006X is heavily extinguished, perhaps by circumstellar dust (Patat et al. 2007; Wang et al. 2008a). Thus, the physical origin of the UV excess in these two SNe Ia might not be the same. In SN 2006X, dust scattering may contribute in part to the unusually bright behavior in the UV, which is favored by the detection of surrounding circumstellar material (Patat et al. 2007) and/or a light echo around this object (Wang et al. 2008b).

We further emphasize here the significance of the discovery of a UV excess in SN 2004dt. It not only provides a new clue to the study of SN Ia physics and/or the progenitor environments but also draws attention to another possible systematic error that might exist in current cosmological studies: the relatively higher UV flux would result in a bluer $U-B$ color for some SNe Ia, which could lead to an underestimate of the host-galaxy reddening and hence an overestimate of the distance. It is of interest to determine the fractional population of the SN 2004dt-like events or those showing a UV excess in both the local and distant universe and to estimate the impact of such a peculiar subclass of SNe Ia on current cosmological results.

We thank Mark Sullivan and Andy Howell for their suggestions. Financial support for this work has been provided by the National Science Foundation of China (NSFC grants 11178003, 11073013, and 10173003) and the National Key Basic Research Science Foundation (NKBRSF TG199075402). A.V.F.'s group at U.C. Berkeley is grateful for the support of NSF grants AST-0607485 and AST-0908886, the TABASGO Foundation, and US Department of Energy grants DE-FC02-06ER41453 (SciDAC) and DE-FG02-08ER41563. Substantial financial support for this work was also provided by NASA through grants GO-10182, AR-12126, and AR-12623 from the Space Telescope Science Institute, which is operated by Associated Universities for Research in Astronomy, Inc., under NASA contract NAS 5-26555. The work of L.W. is supported by NSF grant AST-0708873. J.C.W. is supported by NSF grant AST-0707769. K.N. is supported by WPI Initiative, MEXT, Japan. M.T., S.B., and E.C. are supported by grant ASI-INAF I/009/10/0. P.A.M. is supported by NASA ADP NNX06AH85G. The work of M.H. is supported by ICM grant P10-064-F and CONICYT grants 150100003 and PFB-06, Chile.

REFERENCES

Altavilla, G., Stehle, M., Ruiz-Lapuente, P., et al. 2007, A&A, 475, 585
Arnett, W. D. 1982, ApJ, 253, 785
Benetti, S., Cappellaro, E., Mazzali, P. A., et al. 2005, ApJ, 623, 1011
Bongard, S., Baron, E., Smadja, G., et al. 2008, ApJ, 687, 456
Branch, D., Dang, L., & Baron, E. 2009, PASP, 121, 238
Branch, D., Dang, L. C., Hall, N., et al. 2006, PASP, 118, 560
Branch, D., Doggett, J. B., Nomoto, K., & Thielemann, F.-K. 1985, ApJ, 294, 619
Branch, D., Fisher, A., & Nugent, P. 1993, AJ, 106, 2383
Branch, D., & Venkatakrishna, K. L. 1986, ApJ, 306, L21
Brown, P. J., Dawson, K. S., de Pasquale, M., et al. 2011, (arXiv:1110.2538)
Brown, P. J., Roming, P. W. A., Milne, P., et al. 2010, ApJ, 721, 1608
Bufano, F., Immler, S., Turatto, M., et al. 2009, ApJ, 700, 1456
Cardelli, J. A., Clayton, G. C., & Mathis, J. S. 1989, ApJ, 345, 245
Chiaberge, M., & Sirianni, M. 2007, Instrument Science Report ACS 2007-03
Contreras, C., Hamuy, M., Phillips, M. M., et al. 2010, AJ, 139, 519
Cooke, J., Ellis, R. S., Sullivan, M., et al. 2011, ApJ, 727, L35
Ellis, R. S., Sullivan, M., Nugent, P. E., et al. 2008, ApJ, 674, 51
Filippenko, A. V. 1997, ARA&A, 35, 309
Filippenko, A. V., Richmond, M. W., Branch, D., et al. 1992a, AJ, 104, 1543
Filippenko, A. V., Richmond, M. W., Matheson, T., et al. 1992b, ApJ, 384, L15
Foley, R. J., Challis, P. J., Filippenko, A. V., et al. 2011, ApJ, 744, 38
Foley, R. J., Filippenko, A. V., & Jha, S. W. 2008, ApJ, 686, 117
Foley, R. J., Filippenko, A. V., Kessler, R., et al. 2012, AJ, in press (arXiv:1010.2749)
Foley, R. J., & Kasen, D. 2011, ApJ, 729, 55
Ganeshalingam, M., Li, W., & Filippenko, A. V. 2011, MNRAS, 416, 2607
Ganeshalingam, M., Li, W., Filippenko, A. V., et al. 2010, ApJS, 190, 418
Garavini, G., Nobili, S., Taubenberger, S., et al. 2007, A&A, 471, 527
Gerardy, C., Höflich, P., Fesen, R. A., et al. 2004, ApJ, 607, 391
Goldhaber, G., Groom, D. E., Kim, A., et al. 2001, ApJ, 558, 359
Goobar, A. 2008, ApJ, 686, L103
Guy, J., Astier, P., Baumont, S., et al. 2007, A&A, 466, 11
Hicken, M., Challis, P., Jha, S., et al. 2009, ApJ, 700, 331
Höflich, P., Krisciunas, K., Khokhlov, A. M., et al. 2010, ApJ, 710, 444
Höflich, P., Wheeler, J. C., & Thielemann, F.-K. 1998, ApJ, 495, 617
Howell, A., Sullivan, M., Brown, E. F., et al. 2009, ApJ, 691, 661
Howell, A., Sullivan, M., Nugent, P. E., et al. 2006, Nature, 443, 308
Hsiao, E. Y., Conley, A., Howell, D. A., et al. 2007, ApJ, 663, 1187
Immler, S., Brown, P. J., Milne, P., et al. 2006, ApJ, 648, L119
Jack, D., Hauschildt, P. H., & Baron, E. 2009, A&A, 502, 1043
Jack, D., Hauschildt, P. H., & Baron, E. 2011, A&A, 528, 141
Kasen, D. 2006, ApJ, 649, 939
Kasen, D., Röpke, F. K., & Woosley, S. E. 2009, Nature, 460, 7257
Kelly, P. L., Hicken, M., Burke, D. L., Mandel, K. S., & Kirshner, R. P. 2010, ApJ, 715, 743
Kessler, R., Becker, A. C., Cinabro, D., et al. 2009, ApJS, 185, 32
Kirshner, R. P., Jeffery, D. J., Leibundgut, B., et al. 1993, ApJ, 415, 589
Kromer, M., & Sim, S. A. 2009, MNRAS, 398, 1809
Kümmel, M., Walsh, J., Larsen, S., & Hook, R. 2004, ST-ECF Newsl., 36, 10
Kümmel, M., Walsh, J. R., Pirzkal, N., Kuntschner, H., & Pasquali, A. 2009, PASP, 121, 59
Lampeitl, H., Smith, M., Nichol, R. C., et al. 2010, ApJ, 722, 566
Larsen, S. S., Walsh, J., & Kümmel, M. 2006, ST-ECF Instrument Science Report ACS-2006-03
Leibundgut, B., Kirshner, R. P., Phillips, M. M., et al. 1993, AJ, 105, 301
Lentz, E. J., Baron, E., Branch, D., Hauschildt, P. H., & Nugent, P. E. 2000, ApJ, 530, 966
Leonard, D. C., Li, W., Filippenko, A. V., Foley, R. J., & Chornock, R. 2005, ApJ, 632, 450
Li, W., Filippenko, A. V., Chornock, R., et al. 2003, PASP, 115, 453
Livio, M., & Pringle, J. E. 2011, ApJ, 740, L18
Maeda, K., Benetti, S., Stritzinger, M., et al. 2010, Nature, 466, 82
Maeda, K., Leloudas, G., Taubenberger, S., et al. 2011, MNRAS, 413, 3075
Maund, J. R., Höflich, P., Patat, F., et al. 2010, ApJ, 725, L167
Mazzali, P. A. 2000, A&A, 363, 705
Mazzali, P. A., Benetti, S., Altavilla, G., et al. 2005, ApJ, 623, L37
Milne, P. A., Brown, P. J., Roming, P. W. A., et al. 2010, ApJ, 721, 1627
Nomoto, K., Thielemann, F.-K., & Yokoi, K. 1984, ApJ, 286, 644
Oke, J. B., & Sandage, A. 1968, ApJ, 154, 21
Panagia, N. 2003, in Supernovae and Gamma-Ray Bursters, ed. K. Weiler (Berlin: Springer), 113
Panagia, N. 2007, in AIP Conf. Proc. 937, Supernova 1987A: 20 Years After, ed. S. Immler, R. McCray, & K. W. Weiler (New York: AIP), 236
Patat, F., Baade, D., Höflich, P., et al. 2009, A&A, 508, 229
Patat, F., Chandra, P., Chevalier, R., et al. 2007, Science, 317, 924
Pauldrach, A. W. A., Duschinger, M., Mazzali, P. A., et al. 1996, A&A, 312, 525
Pavlovsky, C. I., Biretta, J., Bohlin, R., et al. 2004, ACS Instrument Handbook, Version 5.0 (Baltimore, MD: STScI)
Perlmutter, S., Gabi, S., Goldhaber, G., et al. 1997, ApJ, 483, 565
Phillips, M. M. 1993, ApJ, 413, L105
Phillips, M. M., Lira, P., Suntzeff, N. B., et al. 1999, AJ, 118, 1766

Phillips, M. M., Wells, L. A., Suntzeff, N. B., et al. 1992, AJ, 103, 1632
Reindl, B., Tammann, G. A., Sandage, A., & Saha, A. 2005, ApJ, 624, 532
Riess, A. G., Macri, L., Casertano, S., et al. 2009, ApJ, 699, 539
Riess, A. G., Press, W. H., & Kirshner, R. P. 1996, ApJ, 473, 588
Sauer, D., Mazzali, P. A., Blondin, S., et al. 2008, MNRAS, 391, 1605
Schlegel, D. J., Finkbeiner, D. P., & Davis, M. 1998, ApJ, 500, 525
Silverman, J. M., Foley, J. R., Filippenko, A. V., et al. 2012, MNRAS, submitted (arXiv:1202.2128)
Silverman, J. M., Ganeshalingam, M., Li, W., et al. 2011, MNRAS, 410, 585
Sim, S. A., Röpke, F. K., Hillebrandt, W., et al. 2010, ApJ, 714, L52
Sirianni, M., Jee, M. J., Benítez, N., et al. 2005, PASP, 117, 1049
Stanishev, V., Goobar, A., Benetti, S., et al. 2007, A&A, 469, 645
Stritzinger, M., & Leibundgut, B 2005, A&A, 431, 423
Sullivan, M., Conley, A., Howell, D. A., et al. 2010, MNRAS, 406, 782
Sullivan, M., Ellis, R. S., Howell, D. A., et al. 2009, ApJ, 693, L76
Tanaka, M., Mazzali, P. A., Benetti, S., et al. 2008, ApJ, 677, 448
Taubenberger, S., Benetti, S., Childress, M., et al. 2011, MNRAS, 412, 2735
Thomas, R. C. 2005, IAU Circ., 8474
Timmes, F. X., Brown, E. F., & Truran, J. W. 2003, ApJ, 590, L83
Wang, L. 2005, ApJ, 635, L33
Wang, L., Baade, D., Höflich, P., et al. 2006a, ApJ, 653, 490
Wang, L., Baade, D., & Patat, F. 2007, Science, 315, 212
Wang, X., Filippenko, A. V., Ganeshalingam, M., et al. 2009a, ApJ, 699, L139 (W09a)
Wang, X., Li, W., Filippenko, A. V., et al. 2008a, ApJ, 675, 626
Wang, X., Li, W., Filippenko, A. V., et al. 2008b, ApJ, 677, 1060
Wang, X., Li, W., Filippenko, A. V., et al. 2009b, ApJ, 697, 380 (W09b)
Wang, X., Wang, L., Pain, R., Zhou, X., & Li, Z. 2006b, ApJ, 645, 488
Zhang, T., Wang, X., Li, W., et al. 2010, PASP, 122, 1